

AGU Advances

RESEARCH ARTICLE

10.1029/2025AV001737

Peer Review The peer review history for this article is available as a PDF in the Supporting Information.

Key Points:

- The warming of the Southern Hemisphere (SH) subtropical lower stratosphere over 2002–2022 is linked to a Brewer-Dobson Circulation slowdown
- These circulation changes cool the Antarctic lower stratosphere and mask the Antarctic ozone healing from October to December
- Removing circulation changes eliminates SH subtropical stratospheric warming and reveals Antarctic warming and enhanced ozone healing

Supporting Information:

Supporting Information may be found in the online version of this article.

Correspondence to:

A. Sweeney and Q. Fu,
aodhan@uw.edu;
qfu@uw.edu

Citation:

Sweeney, A., Fu, Q., Solomon, S., Po-Chedley, S., Randel, W. J., Steiner, A., et al. (2025). Recent warming of the southern Hemisphere subtropical lower stratosphere and Antarctic ozone healing. *AGU Advances*, 6, e2025AV001737. <https://doi.org/10.1029/2025AV001737>

Received 14 MAR 2025

Accepted 24 JUN 2025

Author Contributions:

Conceptualization: Aodhan Sweeney, Qiang Fu

Formal analysis: Aodhan Sweeney, Qiang Fu, Susan Solomon, Stephen Po-Chedley, William J. Randel, Andrea Steiner, Pu Lin, Thomas Birner, Sean Davis, Peidong Wang

Funding acquisition: Aodhan Sweeney, Qiang Fu

Investigation: Aodhan Sweeney, Qiang Fu, Susan Solomon, Stephen Po-

© 2025. The Author(s).

This is an open access article under the terms of the [Creative Commons Attribution License](#), which permits use, distribution and reproduction in any medium, provided the original work is properly cited.

Recent Warming of the Southern Hemisphere Subtropical Lower Stratosphere and Antarctic Ozone Healing

Aodhan Sweeney¹ , Qiang Fu¹ , Susan Solomon² , Stephen Po-Chedley³ , William J. Randel⁴ , Andrea Steiner⁵, Pu Lin⁶ , Thomas Birner^{7,8} , Sean Davis⁹ , and Peidong Wang² 

¹Department of Atmospheric and Climate Science, University of Washington, Seattle, WA, USA, ²Department of Earth, Atmospheric, and Planetary Sciences, Massachusetts Institute of Technology, Cambridge, MA, USA, ³Program for Climate Model Diagnosis and Intercomparison, Lawrence Livermore National Laboratory, Livermore, CA, USA, ⁴NSF National Center for Atmospheric Research, Boulder, CO, USA, ⁵Wegener Center for Climate and Global Change, University of Graz, Graz, Austria, ⁶Program in Atmospheric and Oceanic Sciences, Princeton University, Princeton, NJ, USA, ⁷Meteorological Institute, Ludwig-Maximilians-Universität München, Munich, Germany, ⁸Institute of Atmospheric Physics, Deutsches Zentrum für Luft- und Raumfahrt, Oberpfaffenhofen, Germany, ⁹NOAA Chemical Sciences Laboratory, Boulder, CO, USA

Abstract Observed temperature changes from 2002 to 2022 reveal a pronounced warming of the Southern Hemisphere (SH) subtropical lower stratosphere, and a cooling of the Antarctic lower stratosphere. In contrast, model simulations of 21st-century stratospheric temperature changes show widespread cooling driven by increasing greenhouse gases, with local warming in the Antarctic lower stratosphere due to ozone healing. We provide evidence that these discrepancies between observed and simulated stratospheric temperature changes are linked to a slowdown of the Brewer-Dobson Circulation, particularly in the SH. These changes in the stratospheric circulation are strongest from October through December. This altered circulation warms the SH subtropical lower stratosphere while cooling the Antarctic lower stratosphere, canceling and even reversing the Antarctic ozone recovery that would have occurred in its absence during this period. When circulation changes are accounted for, the SH subtropical lower-stratospheric warming is removed, and Antarctic lower-stratospheric warming is revealed with enhanced ozone healing, highlighting the crucial role of the stratospheric circulation in shaping temperature and ozone changes.

Plain Language Summary Climate models predict that rising greenhouse gas levels cool the stratosphere, while the healing of the Antarctic ozone hole—driven by the reduction of ozone-depleting substances under the Montreal Protocol since the beginning of the 21st century—should warm the Antarctic lower stratosphere. However, observations for the period from 2002 to 2022 reveal unexpected changes: warming in the Southern Hemisphere (SH) subtropical lower stratosphere and cooling over Antarctica. This study identifies the cause as a slowdown in stratospheric circulation that moves stratospheric air and chemicals from low to high latitudes. These circulation changes, most pronounced from October to December, lead to warming in the subtropical lower stratosphere of the SH and cooling in the Antarctic lower stratosphere. They also mask the anticipated ozone recovery over Antarctica during this period. Accounting for these circulation changes removes the anomalous warming of the SH subtropical lower stratosphere and reveals an obvious Antarctic lower stratospheric warming and enhanced ozone recovery. These findings highlight the crucial role of the stratospheric circulation in shaping temperature and ozone changes.

1. Introduction

Observations largely confirm the expected response to increased greenhouse gas concentrations (GHGs) of tropospheric warming and stratospheric cooling (e.g., Fu et al., 2004; Karoly et al., 1994; Khaykin et al., 2017; Ladstädter et al., 2023; Manabe & Wetherald, 1967; Santer et al., 2023; Steiner, Ladstädter, Ao, et al., 2020; Vallis et al., 2015). However, from 2002 to 2022, an unexpected anomalous warming of the Southern Hemisphere (SH) subtropical lower stratosphere was found in Radio Occultation (RO) observations (see Figure 1a) (Gleisner et al., 2022; IPCC, 2023; Ladstädter et al., 2023; Shangguan et al., 2019). The underlying cause of this Anomalous Warming of the Lower Stratosphere (abbreviated as AWLS) remains unknown.

Chedley, William J. Randel,
Andrea Steiner, Pu Lin, Thomas Birner,
Sean Davis, Peidong Wang

Methodology: Aodhan Sweeney,
Qiang Fu, Susan Solomon

Project administration:

Aodhan Sweeney, Qiang Fu

Resources: Aodhan Sweeney, Qiang Fu

Software: Aodhan Sweeney, Stephen Po-Chedley

Supervision: Qiang Fu, Susan Solomon

Validation: Aodhan Sweeney

Visualization: Aodhan Sweeney,

Qiang Fu, Susan Solomon, Stephen Po-Chedley

Writing – original draft:

Aodhan Sweeney

Writing – review & editing:

Aodhan Sweeney, Qiang Fu,

Susan Solomon, Stephen Po-Chedley,

William J. Randel, Andrea Steiner, Pu Lin,
Thomas Birner, Sean Davis,

Peidong Wang

Over the same period, the observed Antarctic lower stratosphere cooled in contrast to the expected warming induced by ozone recovery (Fu et al., 2019; Hu et al., 2011; Ladstädter et al., 2023; Maycock, 2016; Maycock et al., 2018; Randel et al., 2017; Solomon et al., 2017). Observed warming in the AWLS region and cooling in the Antarctic lower stratosphere vary seasonally, but the largest changes in both regions occur from October–December (Ladstädter et al., 2023). This observed dipolar change in lower stratospheric temperature between the subtropical SH and Antarctic might be evidence for changes in the SH Brewer-Dobson Circulation (BDC) which can link variability between the low and high latitude stratosphere (Butchart, 2014).

The BDC plays a crucial role in regulating the distribution and transport of ozone, which is produced at lower latitudes and moved poleward by the circulation (Brewer, 1949; Dobson, 1956; Perliski et al., 1989). The SH-BDC can also change the temperature of the Antarctic stratospheric vortex, which determines the efficiency of chemical ozone depletion (Solomon et al., 1986; World Meteorological Organization Executive Summary, 2022). While Antarctic ozone healing since 2000 has been detected during September in line with model simulations, recovery from October to December is not observed (e.g., see Figures 4–16 in World Meteorological Organization Executive Summary, 2022; Solomon et al., 2016; Solomon et al., 2017; Wang et al., 2025; Chipperfield & Bekki, 2024; Chipperfield et al., 2017; Kuttippurath & Nair, 2017; Stone et al., 2021; Kessenich et al., 2023). Dynamical activity during these months strongly impacts temperature and ozone changes (e.g., Dhomse et al., 2018; Randel & Wu, 2015; Robertson et al., 2023). In addition, enhanced aerosol loadings and chemical processes related to wildfires and volcanoes may also contribute to the discrepancies (e.g., Bernath et al., 2022; Solomon et al., 2022; Solomon et al., 2023; Stocker et al., 2021; Stocker et al., 2024; Stone et al., 2021; Wang et al., 2023; Yook et al., 2022; Zhang et al., 2024). Recently, Wang et al. (2025) demonstrated a striking agreement in the observed and simulated fingerprint pattern of Antarctic ozone response to decreasing ozone depleting substances (ODSs) since 2005, offering strong evidence that Antarctic ozone recovery is underway. They also discovered that ODS forcing has amplified the Antarctic ozone internal variability during austral spring compared to the pre-ODS era, affecting the detection of ozone recovery.

Here we show that the AWLS is linked to a slowdown of the BDC, particularly in the SH. We focus mainly on 2002–2022 but also consider other time periods. These circulation changes not only warm the AWLS region but also cool the Antarctic lower stratosphere. We also explore the implications of this SH-BDC slowdown for ozone and indicate that it can obscure signs of Antarctic ozone healing from October to December, depending on the time period considered. While external forcing associated with GHGs and ODSs remains relatively stable regardless of the chosen time periods, internal variability is highly sensitive to start and end dates as well as the duration of the period. By accounting for this decadal variation in the BDC, we bring observed and simulated temperature and ozone changes for 2002–2022 into an overall agreement.

Section 2 describes the data and methods used. In Section 3, we first partition temperature changes from 2002 to 2022 into those related to the AWLS and those that are not. We then investigate the seasonal variation of temperature and ozone changes, as well as the influence of the stratospheric circulation on these changes, followed by a comparison with simulated changes from a representative climate model. The discussion and sensitivity analysis in Section 4 establishes context for our findings. Finally, Section 5 summarizes our results and highlights their importance.

2. Data and Methods

We analyze interannual variability and decadal trends of stratospheric variables using monthly anomalies, calculated by removing the 2002–2022 monthly climatology from the monthly mean data. We removed interannual variability associated with the El Niño Southern Oscillation (ENSO) and the Quasi-Biennial Oscillation (QBO) using a multiple linear regression (MLR), which was fitted to the anomalies of stratospheric variables and then subtracted (Randel & Wu, 2015; Steiner, Ladstädter, Randel, et al., 2020; Steiner, Ladstädter, Ao, et al., 2020; Tseng & Fu, 2017). ENSO is represented by the MEI-V2 index with a 3-month lead to maximize its impact on the lower stratosphere (Ladstädter et al., 2023; Wolter & Timlin, 2011), and QBO is represented by the first two principal components of Singapore wind observations (Wallace et al., 1993). All results presented in this study have these modes of variability removed.

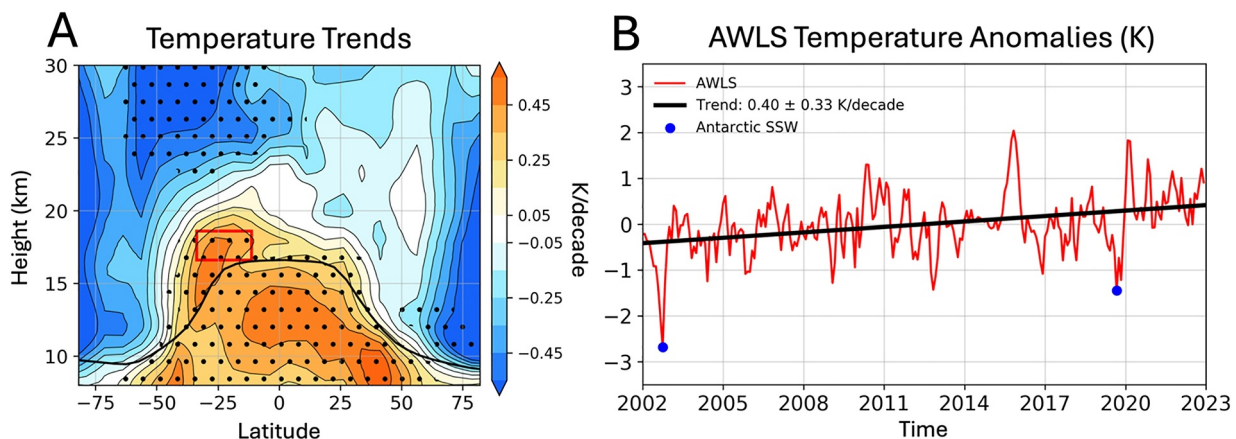


Figure 1. (a) Zonal-mean temperature trends from 8 to 30 km during 2002–2022 derived from Radio Occultation data using anomalies from all months. Stippling indicates statistically significant trends at 95% confidence. The climatological lapse-rate tropopause height is indicated by the thick black line. The red box highlights the region with the Anomalous Warming of the Lower Stratosphere (AWLS). (b) Monthly temperature anomaly timeseries in the AWLS region (i.e., the red box of panel (a)).

2.1. Observation and Reanalysis Data Sets

This analysis uses observations of atmospheric temperature and trace gas species. Observations of temperature come from RO measurements stored by the COSMIC Data Analysis and Archive Center (CDAAC) from 2002 to 2022. RO temperature measurements provide stable and accurate temperature observations of the upper-troposphere and lower-stratosphere (UTLS) region with high vertical resolution, allowing for detailed investigation of changes in this region (Khaykin et al., 2017; Kuo et al., 2004; Kursinski et al., 1997; Leroy et al., 2018; Scherlin-Pirscher et al., 2021; Steiner et al., 2013, Steiner, Ladstädter, Randel, et al., 2020). Data was pre-processed using the level 2 DryPrf from all RO satellites. RO temperature profiles were binned into monthly-mean, zonal-mean temperature fields with 200 m vertical resolution and 7.5° latitudinal resolution.

Observations of stratospheric ozone and water vapor come from SWOOSH, a merged record derived from limb soundings and solar occultations spanning 1984 to present (Davis et al., 2016). We use SWOOSH V2.7 data from 2002 to 2022, which relies heavily on measurements from the Microwave Limb Sounder onboard the Aura satellite, launched in 2004 (Livesey et al., 2021; Read et al., 2007). The primary SWOOSH product used here is the monthly-mean, zonal-mean ozone and water vapor mixing ratios provided on pressure levels. Observed changes in GHGs and chlorofluorocarbons (CFCs) come from the NOAA/ESRL Global Monitoring Laboratory archive based on the Mauna Loa station.

We also use the ERA5 reanalysis data for monthly-mean zonal wind and residual stream functions (replaced by ERA5.1 when available) (Hersbach et al., 2020). Temperature and zonal wind are the monthly average of 6-hourly data at a given latitude and pressure level. The residual stream function is calculated following Diallo et al. (2021) using the 6-hourly data. We also use the monthly mean sea level pressure (SLP) data from ERA5 to calculate the Southern Annular Mode (SAM) index using the first principal component of the 20°–90°S SLP anomalies.

2.2. CESM1 WACCM Simulations

Simulations of the 10-member Community Earth System Model 1 (CESM1) Whole Atmosphere Community Climate Model 4 (WACCM) ensemble are analyzed. These simulations are documented in Zambri et al. (2021) and have GHG concentrations following historical and representative concentration pathway 6.0, and ODS concentrations are prescribed following the WMO (2011) (Meinshausen et al., 2011). These simulations have the same prescribed 28-month QBO and no prescribed solar cycle. Since these simulations have different ENSO and QBO cycles from observations, we create indices to represent these modes in each ensemble. For ENSO, we use the deviation from the ensemble mean of 500 hPa temperature from 15°S to 15°N. For the QBO, we use the ensemble mean zonal wind at 10 and 30 hPa. These three predictors are then fit to each of the ensemble members and removed using a MLR.

2.3. NASA Langley Fu-Liou Radiation Model

We estimate temperature changes due to observed changes in GHGs (CO_2 , CH_4 , N_2O), CFCs, and stratospheric ozone and water vapor through radiative processes by using the NASA Langley Fu-Liou radiation model (Fu & Liou, 1992). Radiatively induced temperature changes are derived using the “Seasonally Evolving Fixed Dynamical Heating” approach, which fixes the dynamical heating so that the resulting temperature changes are the result of radiative processes (Forster and Shine, 1997; Fu et al., 2015; Ming & Hitchcock, 2022). Observed changes in GHGs, CFCs, and stratospheric O_3 and H_2O come from the data sets described in Section 2.1. Changes in well-mixed GHG concentrations are considered throughout the atmosphere, whereas changes in O_3 and H_2O are applied at and above the tropopause. Below the tropopause, water vapor, ozone, and temperature are held to their ERA5 climatological values.

2.4. Trend Calculations

The change for a given variable over a specific time period is quantified using the linear trend derived by applying ordinary least squares regression to the monthly anomalies. Uncertainty estimates for this regression are obtained accounting for the effective degrees of freedom after considering the lag-1 autocorrelation. Significance is defined at the 95% confidence level. Within any given period, the derived linear trend from observations reflects contributions from both external forcing and internal variability.

2.5. Circulation Regression

We aim to partition stratospheric variability into components that covary with temperature in the AWLS region and those that do not. The zonal-mean monthly temperature anomaly timeseries in the AWLS region, referred to as the “AWLS timeseries”, serves as the basis for this partitioning. This method can be applied to any variable of interest, such as temperature, ozone, or zonal wind, using monthly anomalies from all months or from each month individually. To carry out this partitioning, we start with zonal-mean monthly anomalies after removing the QBO and ENSO, which we generically refer to as the “anomalies”, and proceed as follows:

1. Detrend the anomalies at all latitudes (indexed by i) and heights (indexed by j), as well as the AWLS timeseries.
2. Regress the detrended anomalies at each location onto the detrended AWLS timeseries to obtain the regression coefficients, m_{ij} .
3. Multiply m_{ij} by the original (not detrended) AWLS timeseries to obtain the component associated with “circulation variability.” This is referred to as “circulation variability” because m_{ij} is derived from detrended interannual timescales, where stratospheric circulation is the dominant source of variability. Furthermore, as demonstrated later, the trend in the AWLS timeseries is primarily driven by changes in stratospheric circulation.
4. Subtract the circulation variability from the original anomalies to obtain the component that is independent of the AWLS timeseries.

We refer to this technique as the “circulation regression.” Here, we assume that the detrended AWLS timeseries serves as a good proxy for the interannual variability of stratospheric circulation and we provide supporting evidence for this assumption in Section 3.

3. Results

Figure 1a shows the linear trends in zonal mean temperature between 8 and 30 km from the RO record (Steiner, Ladstädter, Ao, et al., 2020). The RO data document a statistically significant warming below the tropopause with tropical tropospheric warming increasing with altitude between 8 and 13 km (Fu et al., 2004; Santer et al., 2005). Most of the stratosphere is cooling, while the AWLS region (highlighted by red box in Figure 1a) shows a strong warming above the SH subtropical tropopause (Gleisner et al., 2022; IPCC, 2021; Khaykin et al., 2017; Ladstädter et al., 2023; Steiner, Ladstädter, Ao, et al., 2020). The AWLS region is defined here as the region between 16.6 and 18.6 km and 33.75° to 11.25°S . Very similar changes are evident in the MSU/AMSU TLS measurements at the same latitudes, suggesting that this warming is not an artifact of RO data (see Figure S1 in Supporting Information S1). Tropopause heights in this region show changes that are not statistically significant, thus the AWLS is unlikely to be a direct manifestation of tropopause height changes (Gao et al., 2015; Weyland

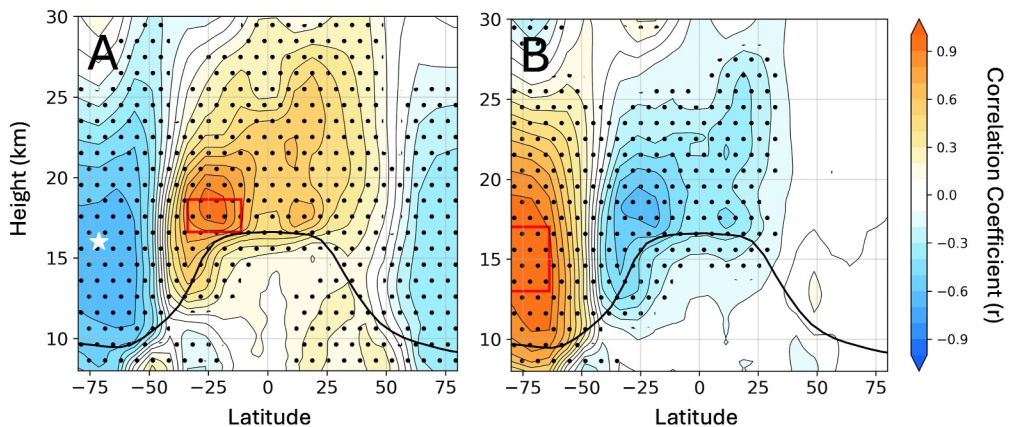


Figure 2. (a) Correlations between the detrended temperature timeseries of the Anomalous Warming of the Lower Stratosphere region and the detrended temperature anomalies from 8 to 30 km. (b) Same as (a), but for the detrended temperature anomalies in the Antarctic lower stratospheric region from 63.7° to 90° S and 13–17 km. Stippling indicates statistically significant correlations. The climatological lapse-rate tropopause height is indicated by the thick black line. The white star shows the location used in Figures 3 and 5.

et al., 2025). Figure 1b shows the monthly temperature anomaly timeseries in the AWLS region, revealing a warming of 0.4 K/decade since 2002 with the 95% confidence interval of ± 0.33 K/decade.

The observed RO temperature changes in Figure 1a also show cooling in the Antarctic. Randel et al. (2017) reported Antarctic warming during 1998–2014 based on both MSU4 observations and WACCM simulations. The contrasting lower-stratospheric temperature trends over Antarctica between the RO observations (Figure 1a) and the WACCM simulations (Figure 9) for 2002–2022 may be attributed to internal variability. Notably, the blue dots in Figure 1b highlight the concurrence of strong negative anomalies in the AWLS region with Antarctic Sudden Stratospheric Warmings (SSWs) in 2002 and 2019 (Lim et al., 2021; Newman & Nash, 2005; Xia et al., 2020). The apparent strong influence of Antarctic SSWs on this subtropical lower stratosphere suggests a close coupling of these regions through the SH-BDC (Zuev et al., 2024). This coupling is exemplified by the correlations between the AWLS region and the Antarctic lower stratosphere shown in Figure 2.

3.1. Partitioning Temperature Changes Based on Covariability With the AWLS

Figure 2a shows the correlation of detrended monthly temperature anomalies from 8 to 30 km with those of the AWLS region. Temperature anomalies in the AWLS region are strongly anticorrelated with those of the Antarctic lower stratosphere. This temperature covariability between the tropical and extratropical lower stratosphere is driven by variability in the BDC (Yulaeva et al., 1994). Figure 2b shows the correlations with detrended temperature anomalies in an Antarctic lower stratospheric region (red box in Figure 2b: 63.75° – 90° S and 13–17 km). In Figure 2b, the region of the strongest anticorrelation with the Antarctic lower stratosphere is the AWLS region, highlighting the coupling of these two regions by the SH-BDC. Here, we emphasize that while the AWLS region was selected for its significant decadal trend (Figure 1), its true importance lies not only in this pronounced trend but, more importantly, in its strong dynamic coupling with the Antarctic lower stratosphere (Figure 2).

The AWLS region exhibits a weaker but significant anticorrelation with the Arctic (Figure 2a), due to the teleconnection between the polar lower stratosphere and the subtropical lower stratosphere in the opposite hemisphere (Figure 2b). Figure S2 in Supporting Information S1 shows an analogous set of correlation maps with the Northern Hemisphere (NH) subtropics and Arctic, revealing similar connections. While this study focuses on the SH and associated stratospheric circulation changes, variations in the NH BDC are an integral part of the overall picture, as discussed in Sections 3.2, 4.2, and 4.5.

Next, we use the circulation regression technique outlined in Section 2.5 to separate stratospheric changes associated with the AWLS timeseries from those that are not. Figure 3 illustrates this for one location in the Antarctic lower stratosphere (71.25° S, 16 km; white star in Figure 2a), which we expect to be coupled to the AWLS via the SH-BDC. The observed temperature anomaly timeseries at this location (Figure 3a) shows an insignificant change of -0.35 ± 1.11 K/decade. Regressing the detrended temperature at this region onto the

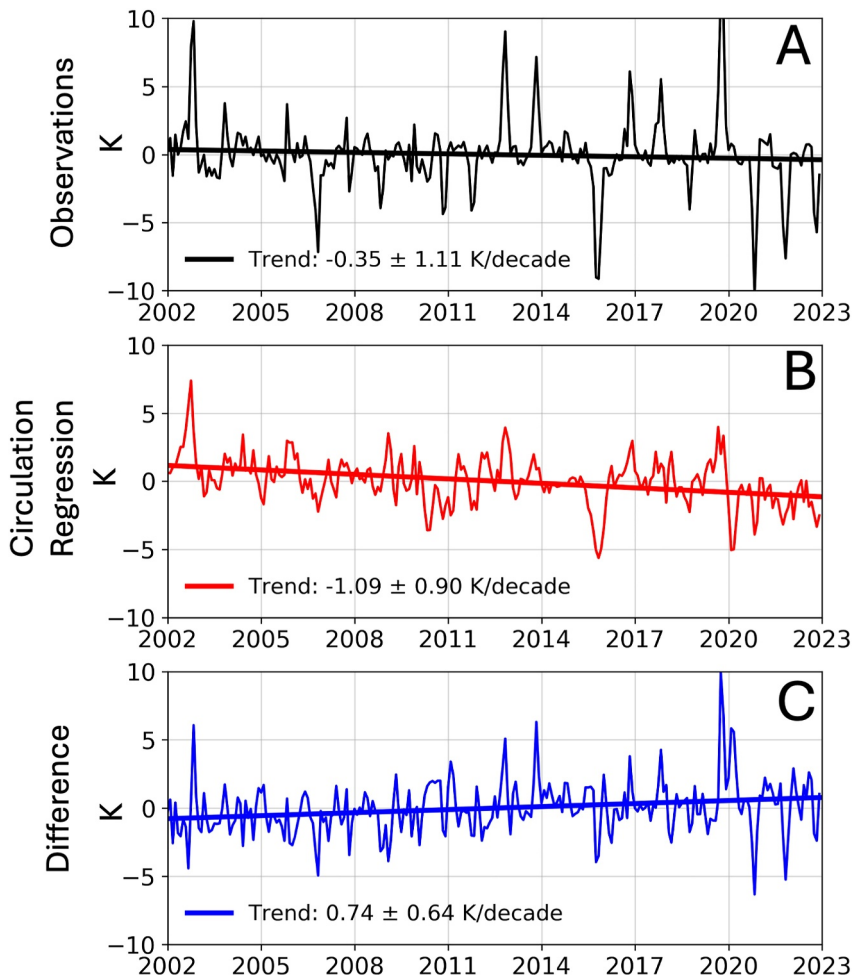


Figure 3. Example of the circulation regression technique applied to temperatures at a specific Antarctic lower stratosphere location (71.25°S , 16 km). (a) RO-observed temperature anomaly timeseries. (b) Circulation regression timeseries, obtained by multiplying the temperature timeseries in the Anomalous Warming of the Lower Stratosphere (AWLS) region by the regression coefficient between the detrended temperature anomalies and the detrended AWLS timeseries. (c) The difference between the observed anomalies (a) and the circulation regression component (b), that is, $c = (a)-(b)$.

detrended AWLS timeseries results in a regression coefficient of -2.73 K/K and a correlation coefficient of -0.66 , revealing strong coupling between these regions. Multiplying this coefficient by the original AWLS timeseries produces the timeseries shown in Figure 3b, which we interpret as representing circulation variability. This timeseries has a statistically significant change of $-1.09 \pm 0.9 \text{ K/decade}$. Figure 3c is the difference after removing covariability with the AWLS from the observed temperature timeseries. This difference timeseries has a statistically significant positive trend and a smaller uncertainty ($0.74 \pm 0.64 \text{ K/decade}$).

The regression coefficient used reflects the interannual coupling between the AWLS and Antarctic, mediated by the SH-BDC. Wang et al. (2025) found that interannual variability of Antarctic lower stratospheric ozone is amplified due to ODSs. This occurs at least in part because interannual variability in the BDC can also influence the efficiency of ozone depletion by modulating polar vortex temperature and location (see Wang et al., 2025 for details). This enhanced ozone variability in turn affects the temperature variability. Figure S3 in Supporting Information S1 shows the ratio of the standard deviation in detrended temperature anomalies between 2002 and 2022 (ODS period) and 1955–1975 (pre-ODS period), based on ERA5 data for (A) January–April (B) May–August, and (C) September–December. It reveals that Antarctic temperature variability during September–December in the ODS period can be up to $\sim 100\%$ higher, supporting Wang et al. (2025). This increased internal variability in both temperature and ozone during this period makes the detection of ozone recovery and its corresponding temperature response more challenging. Since the regression coefficient in the circulation

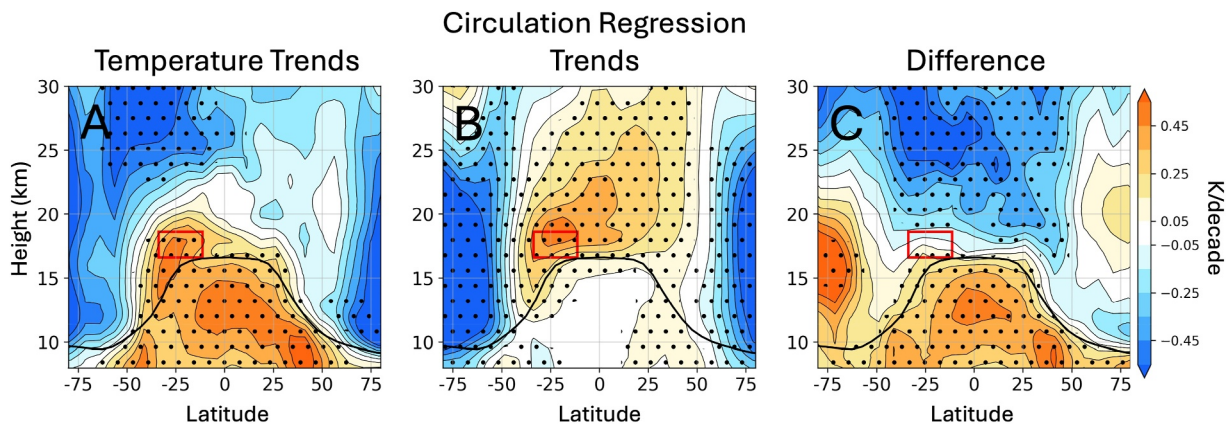


Figure 4. (a) The same as Figure 1a. (b) Trends related to the Anomalous Warming of the Lower Stratosphere based on circulation regression. (c) Difference trend (i.e., (a)–(b)). Stippling in panels A and C indicates areas where trends are statistically significant, while in panel B, stippling shows regions where the regression coefficients from the circulation regression are statistically significant. The tropopause is indicated by the thick black line.

regression is derived from observed interannual variability during 2002–2022, it inherently accounts for the impact of dynamics, chemistry, and radiative interactions on interannual variability during the ODS period.

We now apply the circulation regression to temperatures in the UTLS from 8 to 30 km. Figure 4 presents the results: panel A shows the RO temperature changes from 2002 to 2022 (identical to Figure 1a), panel B displays the temperature changes that are congruent with those in the AWLS region, and panel C illustrates the difference between panels A and B.

The changes related to the AWLS (Figure 4b) exhibit a warming of the tropical lower stratosphere, which hugs the SH subtropical tropopause near the AWLS region, and strong cooling at high latitudes in both hemispheres. This pattern of temperature change in Figure 4b is consistent with a slowdown of the lower-stratospheric BDC (Fu et al., 2019), characterized by reduced upwelling (i.e., less cooling) in the tropics and decreased downwelling (i.e., less warming) in the high latitudes. Because the linear trend of the AWLS timeseries is statistically significant (Figure 1b), the trends in Figure 4b are also statistically significant, as they are derived by multiplying the AWLS timeseries by the corresponding regression coefficients.

Figure 4c presents the temperature change that is not related to the AWLS timeseries, showing strong tropospheric warming and stratospheric cooling, which are the expected atmospheric temperature responses to increased GHGs. In addition, Figure 4c reveals significant warming in the Antarctic lower stratosphere, a feature absent in the observed changes (Figure 4a). This Antarctic lower stratospheric warming is a predicted consequence of ozone healing, as shown in chemistry-climate models, and is expected to peak between September–January near 16 km, mirroring the cooling seen during the ozone depletion era (Fu et al., 2019; Randel et al., 2017; Solomon et al., 2017).

The resemblance between the temperature trend pattern from circulation regression (Figure 4b) and the expected BDC-driven temperature changes reflects our method of isolating these changes using regression coefficients based on interannual variability, which is largely influenced by the BDC. In contrast, the difference panel in Figure 4c aligns with the anticipated temperature response to GHG increases and Antarctic ozone recovery. The similarity of Figure 4c to the expected GHG- and ozone-induced changes suggests that circulation variability is largely internal and has been effectively removed. This reinforces the interpretation that the changes in Figure 4b are primarily due to the stratospheric circulation.

To test whether the AWLS may alternatively be driven by radiative processes, we use the radiative transfer model described in Section 2.3 to estimate the impact of observed atmospheric composition changes on the lower stratospheric temperature (Davis et al., 2016; Forster and Shine, 1997; Fu et al., 2015; Keeling et al., 1976; Lan et al., 2022). Observed changes in radiatively active species, including GHGs, CFCs, and stratospheric O₃, and H₂O, are considered. The results indicate that in response to composition changes, the AWLS region should cool at a rate of -0.18 K/decade. Breaking this down by individual contributions, GHGs and CFCs contribute -0.072 K/decade to the total cooling, while stratospheric O₃ and stratospheric H₂O contribute -0.064 , and

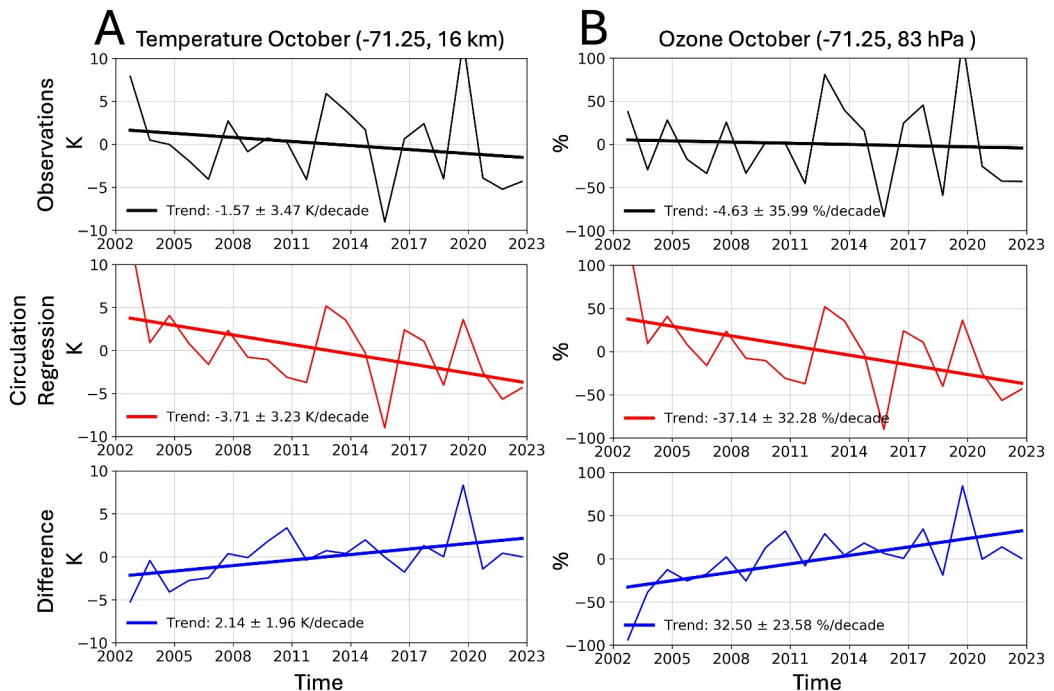


Figure 5. (Black) Timeseries and trends of observed (a) temperature at (71.25°S , 16 km) and (b) ozone at (71.25°S , 83 hPa) in October. (Red) Temperature and ozone timeseries and trends obtained from the monthly circulation regression. (Blue) The difference timeseries and trends after removing the circulation regression component from the observations.

-0.044 K/decade , respectively. While observed changes in stratospheric O_3 and H_2O are also influenced by circulation, the fact that radiative processes would lead to cooling suggests that the pronounced warming of the AWLS region is primarily driven by circulation changes. This strengthens confidence that the decadal variability associated with the AWLS is linked to the circulation trends.

3.2. Seasonality of Temperature Changes

A key finding from Figure 4c is the warming of the Antarctic lower stratosphere consistent with ozone recovery after accounting for circulation variability. However, since Figure 4 shows temperature changes based on anomalies from all months, it does not capture the strong seasonal dependence of ozone recovery. To address this, we apply the circulation regression separately for each month to derive the monthly-resolved circulation impact on temperature changes.

Figure 5a provides an example of the circulation regression applied to the temperature timeseries at a location in the Antarctic stratosphere (white star in Figure 2a), like Figure 3 but applied to the month of October. Observed temperature in October shows an insignificant cooling, with strong interannual variability (black line in Figure 5a). This interannual variability is closely captured by the temperature derived from the circulation regression (red line in Figure 5a), reflecting the strong temperature covariability between the AWLS region and Antarctica. Notably, interannual variability in the AWLS region and the Antarctic location are more strongly correlated during October than in most other months, with a correlation coefficient of -0.86 and a regression coefficient of -4.9 K/K . This is further illustrated in Figure S4 in Supporting Information S1, which presents interannual correlation maps between the AWLS region and the UTLS for each month. Removing circulation variability from October temperature (blue line in Figure 5a) strongly reduces interannual variability and reveals a statistically significant warming trend in the region. The results for ozone (Figure 5b) will be discussed in Section 3.3.

Figure 6 displays temperature trends for 2002–2022 for each month from July–December and shows results from the monthly circulation regression applied to temperatures from 8 to 30 km, while Figure S5 in Supporting Information S1 provides corresponding changes for January to June. Figure 6 row 1 reveals that tropospheric

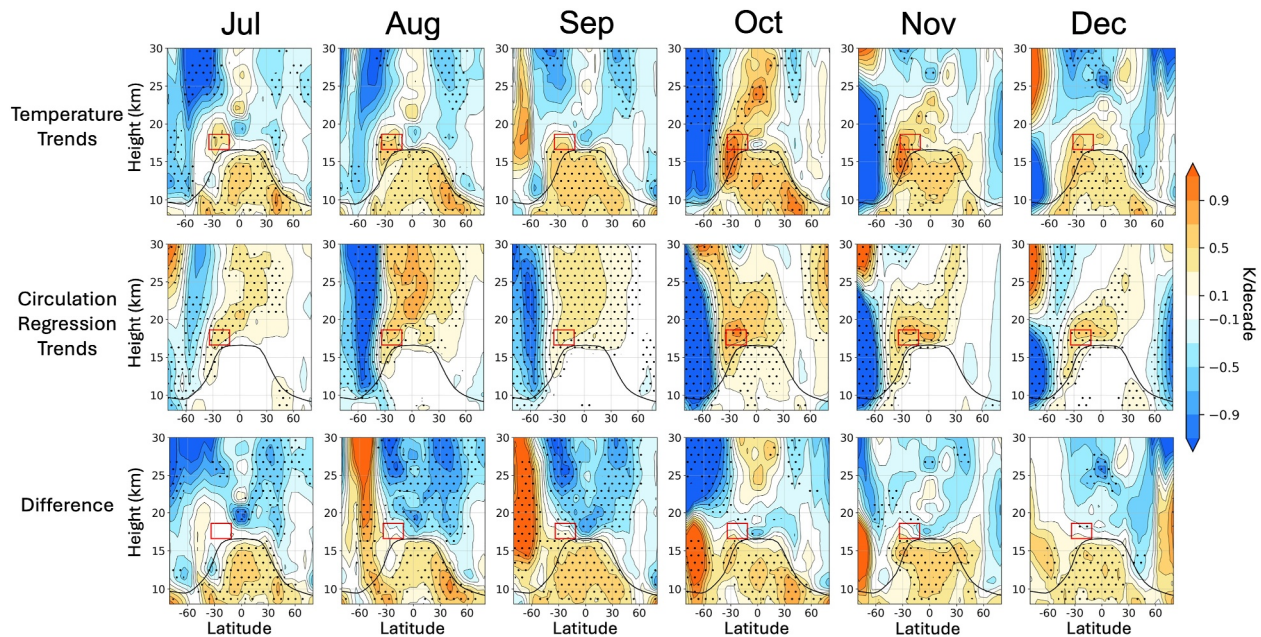


Figure 6. Monthly trends in temperature for the 2002–2022 period. Row 1 shows temperature trends from July to December. Row 2 shows the corresponding trends associated with the Anomalous Warming of the Lower Stratosphere based on the circulation regression. Row 3 shows difference trends (i.e., Row 1 minus Row 2). Stippling in rows 1 and 3 indicates areas where trends are statistically significant, while in row 2, stippling shows regions where the regression coefficients from the circulation regression are statistically significant. The climatological tropopause is indicated by the thick black line.

warming persists year-round, while stratospheric temperature changes depend strongly on season (Khaykin et al., 2017). Figure S6 in Supporting Information S1 presents the monthly AWLS timeseries and changes, indicating consistent warming in the AWLS region throughout the year, with peak warming occurring in October–November and the weakest warming observed in April–May (Ladstädter et al., 2023).

The second row of Figure 6 shows corresponding temperature changes associated with the AWLS, obtained from the monthly circulation regression. Distinct patterns emerge depending on the month, highlighting both the seasonal variation in AWLS magnitude and its relationship to UTLS temperatures. The strongest dipolar coupling between the AWLS region and the Antarctic lower stratosphere occurs from October–December (row 2 of Figure 6). This dipolar pattern during these months closely resembles the circulation-related temperature anomalies identified during the 2002 Antarctic SSW, as documented by Randel and Wu (2015, see their Figure 9). Furthermore, the AWLS during January to April are linked to the Arctic stratosphere (row 2 of Figure S5 in Supporting Information S1).

The third row of Figure 6 presents temperature changes after removing AWLS-related circulation variability. Between August and September, the warming poleward of 50°S intensifies, peaking above 20 km and expanding to cover the polar cap by September. This poleward progression of Antarctic stratospheric warming follows the latitudinal shift of insolation during these months. This warming also descends in altitude, qualitatively aligning with the expected ozone recovery signal in temperature during this period (Solomon et al., 2017; Wang et al., 2025).

After removing AWLS-related changes, an Antarctic warming emerges during September–January (row 3 of Figure 6 and Figure S5 in Supporting Information S1), aligning with the seasonality of ozone recovery (see Sections 3.3; Figure 7). Internal dynamical variability in the SH can hinder the ability to detect signatures of ozone recovery, particularly in October and November (World Meteorological Organization Executive Summary, 2022). However, Figure 6 suggests that removing the circulation effects associated with the AWLS reveals a temperature response consistent with the expected impact of ozone recovery.

Previous studies suggest that during the 21st century, the NH-BDC has slowed more than the SH-BDC above 25 km (Dubé et al., 2025; Ploeger & Garny, 2022). While our circulation regression analysis does not quantify the relative magnitude of the slowdown between the NH and SH-BDC, our results also support a slowdown of the

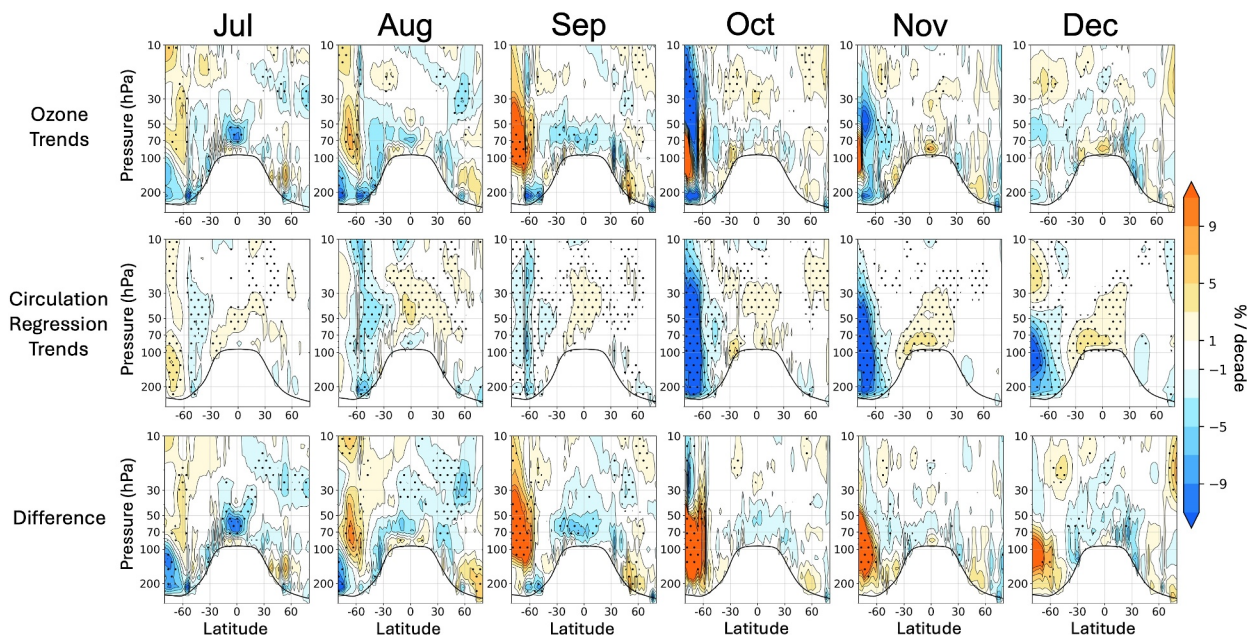


Figure 7. As Figure 6, but for trends in SWOOSH ozone concentration as percent anomaly relative to the 2002–2022 climatology.

NH-BDC for 2002–2022 (Figure 4b and middle panels in Figure S5 in Supporting Information S1 for January–April). Furthermore, Figure 6 and Figure S5 in Supporting Information S1 indicate that the AWLS from January to May is largely linked to the NH-BDC slowdown, while from June to December, it is linked to the SH-BDC slow down. As a result, the SH-BDC and NH-BDC slowdown contributes to the AWLS roughly by 0.27 ± 0.27 K/decade and 0.13 ± 0.13 K/decade, respectively, based on Figure S6 in Supporting Information S1. The former drives the dynamically induced cooling in the Antarctic lower stratosphere.

3.3. Ozone Changes

In this section, we investigate the role of AWLS-related circulation variability in observed stratospheric ozone changes from 2002 to 2022. Figure 5b provides an example of applying the circulation regression to October ozone concentrations in the Antarctic stratosphere at -71.25°S and 83 hPa. Ozone variations are shown as percent anomalies relative to the 2002–2022 monthly climatology, highlighting changes in the lower stratosphere. The black line in Figure 5b represents observed ozone variability, revealing an insignificant change of $-4.63 \pm 35.99\%$ /decade. This result is consistent with Figures 4–16 of the WMO Ozone Assessment Report (World Meteorological Organization Executive Summary, 2022), showing little October total ozone trends over 60° – 90°S since 2000. Regressing interannual October ozone variability at this location onto the detrended AWLS timeseries suggests a strong coupling, with a regression coefficient of $-49\%/\text{K}$ ($r = -0.83$). Notably, the interannual variation of observed ozone (black line in Figure 5b) closely follows that of circulation variability (red line in Figure 5b), which represents the AWLS timeseries multiplied by the regression coefficient. After removing AWLS-related ozone variability, the resulting difference timeseries (blue line in Figure 5b) reveals a significant increase in ozone of $32.5 \pm 23.58\%$ /decade.

The coupling between AWLS temperature and Antarctic ozone (e.g., Figure 5b) can be largely explained by the SH-BDC. Since most high-latitude ozone originates in the lower-latitude stratosphere and is transported poleward by the BDC, a slowdown in the SH-BDC leads to reduced Antarctic ozone concentrations (e.g., Dobson, 1956; Garcia & Solomon, 1983; Orbe et al., 2020; Perliski et al., 1989; Shepherd, 2007). During the ODS period, a weakened SH-BDC further decreases Antarctic ozone by inducing colder Antarctic stratospheric vortices, enhancing chemical ozone depletion and contributing to greater Antarctic ozone interannual variability (Wang et al., 2025). Due to elevated ODS concentrations, a slowdown of the SH-BDC reduces Antarctic ozone through both reduced transport and increased chemical loss due to lower temperatures.

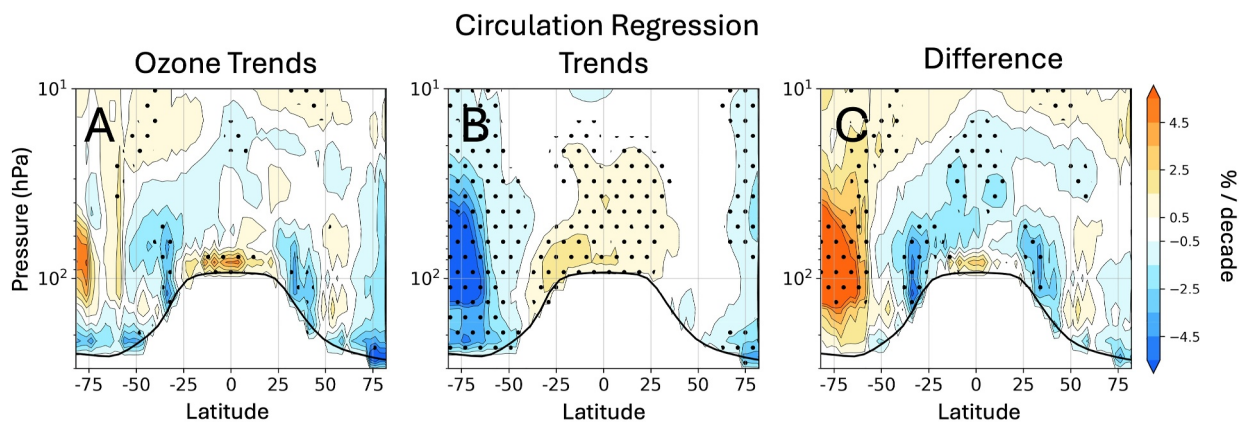


Figure 8. As Figure 4, but for trends in SWOOSH ozone concentration as percent anomaly relative to the 2002–2022 climatology.

We now apply the circulation regression to monthly ozone changes, similar to those applied to temperature in Figure 6. The first row of Figure 7 shows observed changes from July–December for 2002–2022, while changes from January–June are shown in Figure S7 in Supporting Information S1. Observations indicate clear signs of Antarctic ozone healing in September (Solomon et al., 2016); however, changes from October–December primarily show a decline. This decline may result from strong circulation variability, sensitivity to additional forcings not accounted for in the models, and/or observational uncertainties (Chipperfield et al., 2017; Kessenich et al., 2023; Kuttippurath & Nair, 2017; Montzka et al., 2018; Solomon et al., 2016, 2022, 2023; Stone et al., 2021; Villamayor et al., 2023; Yook et al., 2022). In this study, we focus on the role of circulation variability.

The second row of Figure 7 presents the impact of AWLS-related circulation variability on ozone changes. Between October–December, circulation variability decreases Antarctic ozone trends while enhancing positive trends in the tropical lower stratosphere. This dipolar pattern between the tropical and Antarctic lower stratosphere is consistent with a slowdown of the SH-BDC.

The third row of Figure 7 shows ozone changes after removing circulation-driven variability, highlighting a significant increase in Antarctic ozone starting in August. Similar to the temperature changes (row 3 of Figure 6), the observed poleward expansion of the ozone recovery in the Antarctic stratosphere follows the seasonal shift of insolation from August to September. The ozone healing also descends throughout austral spring into summer, aligning with the mean downward motion of polar air due to the BDC, which is an expected feature of ozone healing (Solomon et al., 2017). Overall, the third rows of Figures 6 and 7 suggest that removing AWLS-related changes reveals increases in both temperature and ozone, consistent with the expected effects of ozone recovery (Calvo et al., 2017; Solomon et al., 2016, 2017).

While Figure 7 focuses on monthly ozone changes to identify Antarctic ozone recovery, Figure 8 shows changes calculated from monthly anomalies over all months. In Figure 8a, annual ozone changes from SWOOSH indicate small, insignificant trends in Antarctic ozone poleward of 75°S. Figure 8b displays the annual mean ozone changes associated with AWLS-related circulation variability. Consistent with the monthly ozone analysis, ozone concentrations increase in the tropical lower stratosphere and decrease in the Antarctic, reflecting changes in the SH-BDC. Finally, Figure 8c shows ozone changes after removing the circulation variability, revealing a widespread increase in Antarctic ozone.

3.4. Comparison With Model Simulations

Figure 9a presents ensemble mean temperature changes for 2002–2022 from the CESM1-WACCM 10-member simulations (Zambri et al., 2021). Averaging over the 10 members to obtain the ensemble mean largely mutes the effect of internal variability and provides an estimate of the WACCM simulated forced response over this period. The key differences between the ensemble mean and the observed temperature trend shown in Figure 1a are the minimal warming of the AWLS region and the pronounced warming of the Antarctic lower stratosphere in the simulations (cf., Figures 1a and 9a). Similarly, a comparison of ozone changes reveals a notable difference, with simulations showing a significant recovery of Antarctic ozone (cf., Figures 8a and 9b). Given the influence of

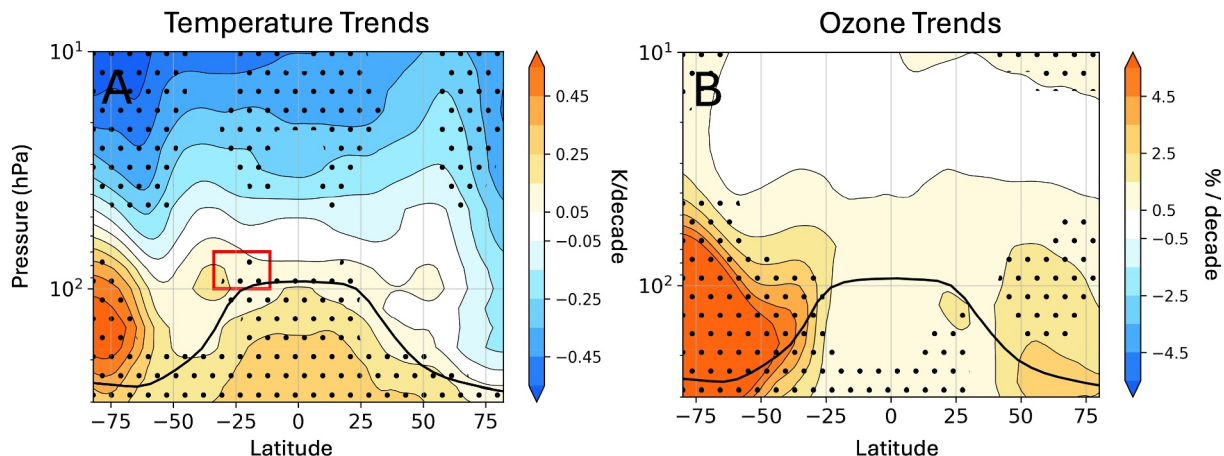


Figure 9. The 10-member ensemble mean of Whole Atmosphere Community Climate Model 4 simulations for (a) temperature and (b) ozone trends for 2002–2022. Stippling and the thick black line follow the same conventions as in Figure 1a.

internal variability, we do not expect strong agreement between observed and simulated ensemble mean changes (see Section 4.7).

Removing circulation variability from observed temperature changes reveals strong warming in the Antarctic lower stratosphere while minimizing warming in the tropical lower stratosphere (see Figure 4c). Similarly, removing circulation variability from ozone changes displays an obvious recovery of Antarctic ozone (Figure 8c). Overall, in both temperature and ozone, accounting for AWLS-related stratospheric circulation results in a better agreement between observed and WACCM simulated changes (cf., 4C and 9A for temperature, and 8C and 9B for ozone). Removing the circulation variability from ozone changes also slightly exacerbates the observed decreases in tropical ozone.

The circulation-adjusted ozone trends in Figure 8c also show significant declines in the subtropical lower stratosphere of both hemispheres, as well as in the tropical region between \sim 15–40 hPa—different from the pattern in Figure 9b. Removing the circulation variability from observed ozone changes thus slightly exacerbates the observed decreases in tropical ozone. These declines persist throughout the year (Figure 7 and Figure S7 in Supporting Information S1), especially from February to June, even before applying the circulation adjustment. Future research is needed to understand why ozone levels are decreasing in these regions despite the reduction in ODS.

Figure S8 in Supporting Information S1 (Figure S9 in Supporting Information S1) shows the monthly temperature (ozone) changes from the WACCM ensemble mean simulations. Like the monthly temperature (ozone) changes after removing circulation variability in the third row of Figure 6 (Figure 7), the WACCM simulations show a seasonally dependent change in Antarctic lower-stratospheric temperature (ozone), which peaks from November–February (October–February). Note that the strongest warming and ozone recovery in this region from the WACCM simulations lag the signals seen in observation (the third row of Figures 6 and 7) by 1–2 months. This may be due to known model biases that delay the breakdown of the SH polar vortex (Butchart et al., 2011; Calvo et al., 2017; Lawrence et al., 2022).

4. Discussion and Sensitivity Analysis

Section 3 suggests that stratospheric circulation changes are a primary driver of observed AWLS and Antarctic lower stratospheric cooling, which also obscure ozone recovery signals in certain months. Removing these circulation effects eliminates the anomalous warming of the SH subtropical lower stratosphere, and reveals Antarctic lower stratospheric warming and ozone recovery. Below we discuss these findings in a broader context.

4.1. Sensitivity to Start and End Dates

Previous studies suggest that excluding years with extreme dynamical variability, or unanticipated forcings (e.g., wildfire, volcanic activity) may help detect ozone recovery (Bernath et al., 2022; Solomon et al., 2022, 2023;

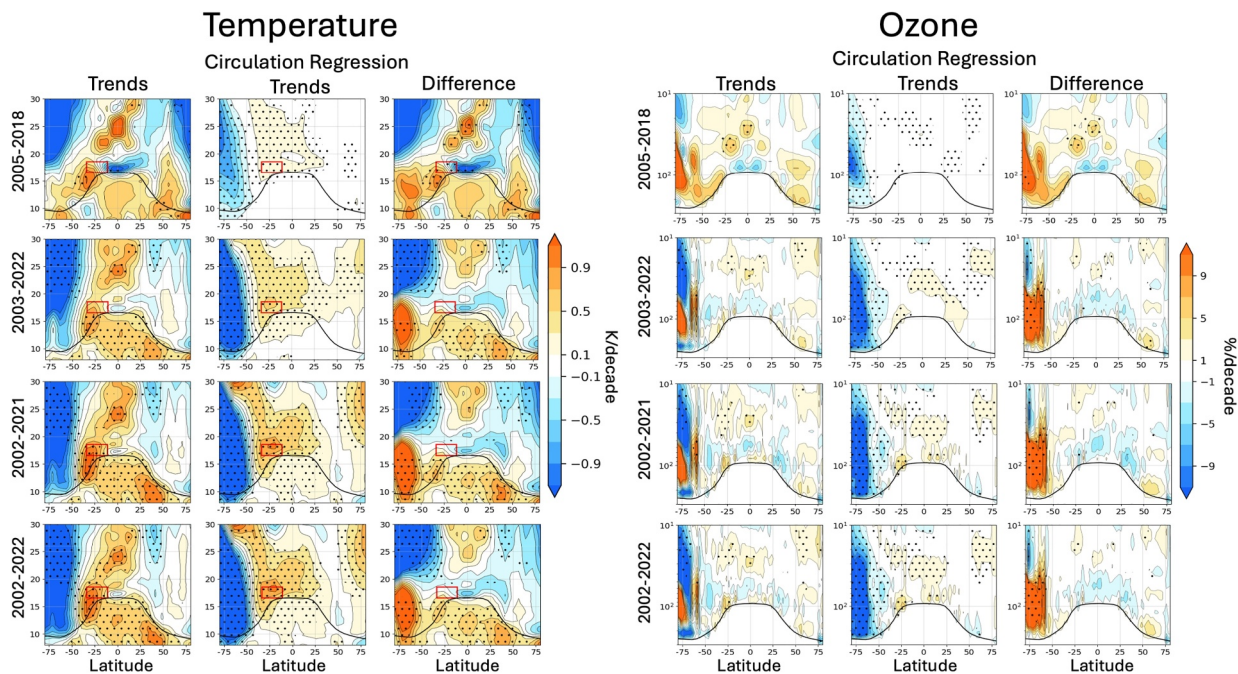


Figure 10. Left (right): Same as Figure 4 (Figure 8) for temperature (ozone) trends but for October during 2005–2018, 2003–2022, and 2002–2021.

Stocker et al., 2021, 2024; Wang et al., 2023; Yook et al., 2022; Zhang et al., 2024). To evaluate the circulation regression's ability to isolate circulation effects, we test its sensitivity to different start and end dates, focusing on October–December. If the method is robust, the changes after removing circulation effects should remain similar regardless of the start and end dates.

Figure 10 presents the temperature (left) and ozone (right) results for October across the periods 2005–2018, 2003–2022, and 2002–2021, in comparison to the full period of 2002–2022. October Antarctic ozone exhibits large interannual variability and is highly influenced by strong dynamical activity (World Meteorological Organization Executive Summary, 2022). Results for November and December are displayed in Figures S10 and S11 in Supporting Information S1. The 2005–2018 period was recently considered in Wang et al. (2025-a) to investigate Antarctic ozone recovery because of minimal impact of extreme dynamics, wildfires, and volcanoes. Interestingly, the observed annual mean AWLS change over this period is 0.1 K/decade, which matches the WACCM ensemble mean warming of 0.1 K/decade there (Figure 9a), suggesting a minimal circulation variability impact. While 2005–2018 circulation variability has some negative impact on October Antarctic temperature and ozone, its impacts are minimal in November and December (Figures S10 and S11 in Supporting Information S1) (Wang et al., 2025-a). Although observed Antarctic temperature and ozone changes remain positive in these months, the October increases become more pronounced after accounting for circulation effects (Figure 10).

For the periods 2003–2022 (excluding the 2002 Antarctic SSW) and 2002–2021 (omitting 2022 to avoid the impact of the Hunga-Tonga eruption), comparisons with the full period 2002–2022 reveal minimal sensitivity to the choice of the start and end years. After removing circulation variability, all periods consistently display Antarctic lower stratospheric warming, and ozone increases—key features of long-term ozone recovery. However, some quantitative differences between 2005 and 2018 and the other periods remain evident, even after removing circulation variability, potentially arising from variations in external forcing, observational uncertainties, and residual effects of circulation variability.

4.2. ERA5 Residual Circulation Changes

If the AWLS is due to changes in the BDC, this should be reflected in residual circulation changes over recent decades. Changes in the ERA5 residual stream function are shown in Figure S12 in Supporting Information S1. Climatological values of the residual stream function are negative in the SH, yet changes show large positive values in this region, suggesting a weakening of the SH-BDC. Note that estimates of the residual circulation

changes might not be well constrained in reanalysis data sets and can vary between products (Ploeger & Garny, 2022; SPARC, 2022). Yet, the different lines of evidence from the circulation regression analysis, radiative transfer calculations, and ERA5 residual stream function changes all point to a dynamically induced AWLS, which can be interpreted as a weakening of the BDC, especially in the SH. Figure S12 in Supporting Information S1 also indicates a weakening of the NH-BDC.

4.3. Relevance to Zonal Wind Changes

Perturbations to the lower-stratospheric temperature gradient associated with the identified circulation variability must align with zonal wind changes through thermal wind balance. In Figure S13 in Supporting Information S1, we partition ERA5 zonal wind changes into those related to the AWLS timeseries and those not related to it by applying the circulation regression to monthly ERA5 zonal wind anomalies (see Section 2.5). The ERA5 zonal wind changes (Figure S13A in Supporting Information S1) show that the stratospheric jet has strengthened in both hemispheres from 2002 to 2022, with the strongest intensification near 50°–60°S. The circulation regression changes show that the AWLS is associated with significant strengthening of the polar stratospheric zonal wind in both hemispheres (Figure S13B in Supporting Information S1). Removing these changes results in small negative and statistically insignificant decadal changes in polar stratospheric zonal wind (Figure S13C in Supporting Information S1), suggesting that the observed stratospheric wind trends are mostly related to the AWLS.

4.4. The Role of the Southern Annular Mode

Changes in the strength and position of the SH stratospheric jet can be understood as variability of the SAM (Fogt & Marshall, 2020; Thompson & Wallace, 2000). This raises the question of whether the circulation variability we identify here is simply a reflection of variability in the SAM. To examine this, we apply an adapted version of the circulation regression to monthly temperature anomalies, by replacing the AWLS timeseries with a SAM index (see Section 2.1 for its definition). The results are shown in Figure S14 in Supporting Information S1. Notably, the AWLS region exhibits a local maximum response to SAM (Figure S14B in Supporting Information S1), further highlighting its dynamic coupling with the Antarctic lower stratosphere. While the pattern of stratospheric temperature changes associated with the SAM (Figure S14B in Supporting Information S1) closely resembles the circulation regression results in Figure 4b, the SAM-related warming in the region of the AWLS is only 0.13 ± 0.1 K/decade, which is $\sim 1/3$ of the 0.4 ± 0.33 K/decade warming trend in the AWLS region (see Figure 1b). This may be partly because the SAM closely tracks the polar vortex strength, which has been strengthened by circulation-driven cooling of the Antarctic stratosphere and weakened by warming due to externally driven ozone healing, leading to a partial cancellation and smaller net changes in the SAM.

4.5. Sensitivity to Box Location as Key Center of BDC Variability

The circulation regression technique (Section 2.5) identified the AWLS region as a key center of SH-BDC variability (Figure 2). While both the SH- and NH-BDC influence the tropical lower stratosphere, using both the AWLS timeseries and the temperature anomaly timeseries of the NH subtropical lower stratosphere (see red box in Figure S2A in Supporting Information S1) has little effect on the results of Figure 4 (not shown). This is because the AWLS timeseries is a good proxy for the NH BDC during January–March, when NH BDC dominates (see Figure S5 in Supporting Information S1). Notably, the detrended AWLS timeseries correlates with its NH counterpart at $r = 0.60$.

Figure S15 in Supporting Information S1 further tests the sensitivity of our results by replacing the AWLS region box with a more conventional “tropical box” spanning 26.25°S to 26.25°N at the same height (Figure 15). While this approach still tracks stratospheric circulation (Figure S15B in Supporting Information S1), it captures less AWLS warming. Difference changes (Figure S15C in Supporting Information S1) recover weak, insignificant Antarctic lower stratospheric warming, and still exhibit strong SH subtropical warming. These results suggest that while the tropical box captures part of variability associated with the stratospheric circulation, it is less indicative of the SH-BDC variability than the selected AWLS region. Notably, the difference change patterns for the NH in Figure 4 and Figure S13 in Supporting Information S1 are nearly identical, indicating that the AWLS region also effectively captures the slowdown of the NH-BDC well (Figures S5 and S12 in Supporting Information S1). Using a “tropical box” spanning 18.75°S to 18.75°N yields very similar results to those in Figure S15 in Supporting Information S1, though the coupling with the poles becomes even weaker.

4.6. Impact of Observational Errors on Circulation Regression Analysis

In the circulation regression analysis, trends unrelated to the circulation are obtained by subtracting circulation variability from the original anomalies. A relevant question is how observational errors affect the trend uncertainty interval of this difference. Suppose the observational errors for the target anomalies and AWLS timeseries are denoted as σ_a and σ_{AWLS} , respectively. The observational error in the difference is then given by $[\sigma_a^2 + (m_{ij} \sigma_{AWLS})^2]^{1/2}$, where m_{ij} is the regression coefficient. This indicates that the observational errors in the difference, which incorporate errors from both the target anomalies and the AWLS timeseries, are larger than those in the original anomalies and circulation variability. However, the trend uncertainty interval of the difference, which is due to both observational errors and interannual variability, remains smaller than that of the original anomalies (Figures 3 and 5). This is because the trend uncertainty is dominated by interannual variability. Since removing circulation variability substantially reduces interannual variability in the difference, it results in a smaller trend uncertainty interval (Figures 3 and 5). Even if the change in the AWLS region for a given month is small and statistically insignificant (Figure S6 in Supporting Information S1), it still significantly contributes to the circulation regression analysis by reducing interannual variability in the difference, thereby narrowing its trend uncertainty interval.

4.7. Circulation Regression Applied to WACCM Simulations

Figure S16a in Supporting Information S1 shows temperature changes from 10 individual WACCM ensemble members over 2002–2022. While Antarctic lower-stratospheric temperature changes vary greatly among members, all members simulate similar weak warming in the AWLS region (ensemble mean: 0.1 K/decade). Since QBO and ENSO effects are removed, these differences primarily reflect internal BDC variability. Figure S16B in Supporting Information S1 shows changes related to each member's AWLS timeseries using circulation regression. Figure S16C in Supporting Information S1 presents the difference changes after removing AWLS-related processes. The similarity between trend patterns in Figures S16A and S16c in Supporting Information S1 indicates that the circulation regression approach is ineffective for model simulations.

Figure S17 in Supporting Information S1 compares simulated and observed R^2 between detrended monthly temperature anomalies in the Antarctic lower stratosphere and UTLS temperatures. Observations show a strong coupling between the Antarctic and AWLS region ($R^2=0.35$), whereas simulations exhibit a much weaker relationship ($R^2=0.15$) across all ensemble members. This suggests that the circulation regression is ineffective for this model's simulations.

4.8. Cause of BDC Changes

Model simulations suggest that two key external drivers of 21st-century BDC changes are rising GHG concentrations and Antarctic ozone recovery (Abalos et al., 2019, 2020, 2021; Garfinkel et al., 2017; Garny et al., 2011; Ivanciu et al., 2022; Lin & Fu, 2013; McLandress et al., 2010, 2011). Increasing GHG levels are expected to accelerate the BDC, causing cooling in the tropical lower stratosphere and warming at the poles—opposite to the observed trends (Figure 1a). In contrast, Antarctic ozone recovery is expected to warm the lower stratosphere over Antarctica, weakening the SH equator-to-pole temperature gradient and inducing a forced slowdown of the SH-BDC (Abalos et al., 2019; Ladstädter et al., 2023; Polvani et al., 2018, 2019). However, this simulated slowdown relies on a significant increase in Antarctic ozone concentration, which would warm the Antarctic. Since such strong increases are absent in observed ozone and temperature changes, the results presented here do not support a forced slowdown of the SH-BDC due to Antarctic ozone recovery.

The WACCM simulation indicates a forced warming of 0.1 K/decade and a radiative component of −0.12 K/decade in the AWLS region, resulting in a forced dynamic component of 0.22 K/decade. Observations, however, indicate a total warming of 0.4 K/decade, with a radiative component of −0.18 K/decade, implying a dynamic component of 0.58 K/decade. This implies that the dynamic component due to internal variability is 0.36 K/decade. Consequently, if we have confidence in the model-simulated forced changes, the 0.4 K/decade (Figure 1b) used in our analysis should largely reflect internal variability.

5. Conclusions

The RO climate record allows for a detailed study of 21st century stratospheric temperature changes (Gleisner et al., 2022; Khaykin et al., 2017; Ladstädter et al., 2023; Mitchell et al., 2020; Shangguan et al., 2019; Steiner, Ladstädter, Ao, et al., 2020; Vergados et al., 2021; Zolghadrshojaee et al., 2024). While models predict widespread stratospheric cooling, RO observations for 2002–2022 show anomalous warming in the SH subtropical lower stratosphere, referred to here as the AWLS. Partitioning temperature changes into those related to the AWLS (Figure 4b) and those that are not (Figure 4c) reveals the influence of stratospheric circulation on temperature changes, distinguishing them from changes driven by rising GHG levels and ozone recovery. This approach remains robust to choices of different time periods (Figure 10, Figures S10 and S11 in Supporting Information S1), reflecting the importance of circulation changes from interannual to decadal timescales for polar temperatures. Seasonal analysis suggests that circulation variability has the strongest impact from October–December. Furthermore, radiative transfer calculations suggest that composition changes alone would lead to cooling in the AWLS region, providing further evidence that warming in this region is circulation driven. Changes in the ERA5 residual stream function also reinforce the evidence for dynamical warming in the AWLS region for 2002–2022. Our findings suggest that the circulation changes identified in this study are largely linked to internal variability rather than to increases in greenhouse gases or reduction in ODSs.

Following the pronounced 20th century ozone depletion, stratospheric ozone concentrations are expected to recover in the 21st century due to the reduction of ODSs (Solomon et al., 2016; World Meteorological Organization Executive Summary, 2022). Detecting robust Antarctic ozone healing is crucial for demonstrating the effectiveness of the Montreal Protocol and its role in mitigating ozone depletion (Barnes et al., 2019; Montzka et al., 2018; Newman et al., 2006; Rigby et al., 2019). While Antarctic ozone healing has been observed during September, October–December ozone healing is less robust (Figure 7). Our findings indicate that the SH-BDC slowdown linked to the AWLS reduces Antarctic ozone concentrations. This is because a weakened SH-BDC reduces poleward ozone transport and creates colder conditions favorable for the chemical depletion of ozone within the Antarctic polar vortex. Our results show that October–December Antarctic ozone recovery would be apparent in observations in the absence of recent circulation influences, consistent with previous studies (Solomon et al., 2016). Overall, we link two previously unconnected discrepancies between models and observations: the AWLS and the weaker-than-expected October–December Antarctic ozone healing.

Future stratospheric climate change will impact surface climate via dynamical and radiative stratosphere-troposphere coupling, thus understanding recent changes in stratospheric dynamics is important (e.g., Butchart, 2014; Haynes et al., 2021). However, constraining the BDC changes over recent decades is difficult, as most BDC metrics are not directly observable and must be inferred from a combination of temperature observations, trace gas measurements, models, and/or reanalysis products (Abalos et al., 2015; Diallo et al., 2021; Fu et al., 2010, 2015, 2019; Mahieu et al., 2014; Ploeger & Gurney, 2022; SPARC, 2022; Stiller et al., 2012; Stiller et al., 2017). This study examines signatures of stratospheric circulation change using temperature provided by high vertical resolution RO data. While temperature is advantageous for studies of BDC change as it is directly observable, analyses using temperature are hindered by the fact that temperature is influenced by both the circulation and radiative processes. This study also calls for further research to investigate the root cause of recent stratospheric circulation changes identified here, which will help reduce uncertainties regarding future changes in stratospheric temperature, composition, and ultimately surface climate.

Conflict of Interest

The authors declare no conflicts of interest relevant to this study.

Data Availability Statement

SWOOSH data is made available by the [NOAA Chemical Sciences Laboratory](#) (Davis et al., 2016). Software and data used to create figures in this manuscript is held on a [zenodo repository](#) (Sweeney, 2025). RO data comes from the [Cosmic Data Analysis and Archive Center](#) website. Monthly ERA5 data comes from the [Climate Data Store](#) (Hersbach et al., 2023).

Acknowledgments

AS and QF were funded by NASA FINESST Grant 80NSSC22K1438 and NSF Grant AGS-2202812. Additional funding was provided by the Calvin Professorship in Atmospheric Sciences. AS's research benefits greatly by attending the GNSS Remote Sensing Colloquium, June 5–16, 2023, in Boulder, Colorado. SS and PW acknowledge support by NSF Grants AGS-2128617 and 2316980. Work by SP was supported by the Regional and Global Model Analysis Program of the Office of Science as part of the PCMDI Project and was performed under the auspices of the U.S. Department of Energy by Lawrence Livermore National Laboratory under Contract DE-AC52-07NA27344. We would like to acknowledge high-performance computing support from Cheyenne (doi:10.5065/D6RX99HX) provided by NCAR's Computational and Information Systems Laboratory, sponsored by the National Science Foundation, for part of the analyses presented in this study and for data management, storage, and preservation. This work was partially completed by the NASA-Aura-ACMAP Science Team under Grant 80NSSC23K1143. We thank Drs. Joel Thornton and Pieter Cornelis Levelt for valuable discussions. We also thank that the processing of the monthly RO record was done by Jon Starr of NCAR.

References

- Abalos, M., Calvo, N., Benito-Barca, S., Garny, H., Hardiman, S. C., Lin, P., et al. (2021). The Brewer–Dobson circulation in CMIP6. *Atmospheric Chemistry and Physics*, 21(17), 13571–13591. <https://doi.org/10.5194/acp-21-13571-2021>
- Abalos, M., Legras, B., Ploeger, F., & Randel, W. J. (2015). Evaluating the advective Brewer–Dobson circulation in three reanalyses for the period 1979–2012. *Journal of Geophysical Research: Atmospheres*, 120(15), 7534–7554. <https://doi.org/10.1002/2015JD023182>
- Abalos, M., Orbe, C., Kinnison, D. E., Plummer, D., Oman, L. D., Jöckel, P., et al. (2020). Future trends in stratosphere-to-troposphere transport in CCM1 models. *Atmospheric Chemistry and Physics*, 20(11), 6883–6901. <https://doi.org/10.5194/acp-20-6883-2020>
- Abalos, M., Polvani, L., Calvo, N., Kinnison, D., Ploeger, F., Randel, W., & Solomon, S. (2019). New insights on the impact of ozone-depleting substances on the brewer-dobson circulation. *Journal of Geophysical Research: Atmospheres*, 124(5), 2435–2451. <https://doi.org/10.1029/2018JD029301>
- Barnes, P. W., Williamson, C. E., Lucas, R. M., Robinson, S. A., Madronich, S., Paul, N. D., et al. (2019). Ozone depletion, ultraviolet radiation, climate change and prospects for a sustainable future. *Nature Sustainability*, 2(7), 569–579. <https://doi.org/10.1038/s41893-019-0314-2>
- Bernath, P., Boone, C., & Crouse, J. (2022). Wildfire smoke destroys stratospheric ozone. *Science*, 375(6586), 1292–1295. <https://doi.org/10.1126/science.abm5611>
- Brewer, A. W. (1949). Evidence for a world circulation provided by the measurements of helium and water vapour distribution in the stratosphere. *Quarterly Journal of the Royal Meteorological Society*, 75(326), 351–363. <https://doi.org/10.1002/qj.49707532603>
- Butchart, N. (2014). The Brewer–Dobson circulation. *Reviews of Geophysics*, 52(2), 157–184. <https://doi.org/10.1002/2013RG000448>
- Butchart, N., Charlton-Perez, A. J., Cionni, I., Hardiman, S. C., Haynes, P. H., Krüger, K., et al. (2011). Multimodel climate and variability of the stratosphere. *Journal of Geophysical Research*, 116(D5), D05102. <https://doi.org/10.1029/2010JD014995>
- Calvo, N., Garcia, R. R., & Kinnison, D. E. (2017). Revisiting southern Hemisphere polar stratospheric temperature trends in WACCM: The role of dynamical forcing. *Geophysical Research Letters*, 44(7), 3402–3410. <https://doi.org/10.1002/2017GL072792>
- Chipperfield, M. P., & Bekki, S. (2024). Opinion: Stratospheric ozone – Depletion, recovery and new challenges. *Atmospheric Chemistry and Physics*, 24(4), 2783–2802. <https://doi.org/10.5194/acp-24-2783-2024>
- Chipperfield, M. P., Bekki, S., Dhomse, S., Harris, N. R. P., Hassler, B., Hossaini, R., et al. (2017). Detecting recovery of the stratospheric ozone layer. *Nature*, 549(7671), 211–218. <https://doi.org/10.1038/nature23681>
- Davis, S. M., Rosenlof, K. H., Hassler, B., Hurst, D. F., Read, W. G., Vömel, H., et al. (2016). The stratospheric water and ozone satellite homogenized (SWOOSH) database: A long-term database for climate studies. *Earth System Science Data*, 8(2), 461–490. <https://doi.org/10.5194/essd-8-461-2016>
- de Forster, P. M. F., & Shine, K. P. (1997). Radiative forcing and temperature trends from stratospheric ozone changes. *Journal of Geophysical Research*, 102(D9), 10841–10855. <https://doi.org/10.1029/96JD03510>
- Dhomse, S. S., Kinnison, D., Chipperfield, M. P., Salawitch, R. J., Cionni, I., Hegglin, M. I., et al. (2018). Estimates of ozone return dates from chemistry-climate model initiative simulations. *Atmospheric Chemistry and Physics*, 18(11), 8409–8438. <https://doi.org/10.5194/acp-18-8409-2018>
- Diallo, M., Ern, M., & Ploeger, F. (2021). The advective Brewer–Dobson circulation in the ERA5 reanalysis: Climatology, variability, and trends. *Atmospheric Chemistry and Physics*, 21(10), 7515–7544. <https://doi.org/10.5194/acp-21-7515-2021>
- Dobson, G. M. B. (1956). Origin and distribution of the polyatomic molecules in the atmosphere. *Proceedings of the Royal Society of London Series A*, 236, 187–193. <https://doi.org/10.1098/rspa.1956.0127>
- Dubé, K., Tegtmeier, S., Ploeger, F., & Walker, K. A. (2025). Hemispheric asymmetry in recent stratospheric age of air changes. *Atmospheric Chemistry and Physics*, 25(2), 1433–1447. <https://doi.org/10.5194/acp-25-1433-2025>
- Fogt, R. L., & Marshall, G. J. (2020). The southern Annular mode: Variability, trends, and climate impacts across the southern Hemisphere. *WIREs Climate Change*, 11(4), e652. <https://doi.org/10.1002/wcc.652>
- Fu, Q., Johanson, C. M., Warren, S. G., & Seidel, D. J. (2004). Contribution of stratospheric cooling to satellite-inferred tropospheric temperature trends. *Nature*, 429(6987), 55–58. <https://doi.org/10.1038/nature02524>
- Fu, Q., Lin, P., Solomon, S., & Hartmann, D. L. (2015). Observational evidence of strengthening of the Brewer–Dobson circulation since 1980. *Journal of Geophysical Research: Atmospheres*, 120(19), 10214–10228. <https://doi.org/10.1002/2015JD023657>
- Fu, Q., & Liou, K. N. (1992). On the correlated k-Distribution method for radiative transfer in nonhomogeneous atmospheres. *Journal of the Atmospheric Sciences*, 49(22), 2139–2156. [https://doi.org/10.1175/1520-0469\(1992\)049<2139:otcdmf>2.0.co;2](https://doi.org/10.1175/1520-0469(1992)049<2139:otcdmf>2.0.co;2)
- Fu, Q., Solomon, S., & Lin, P. (2010). On the seasonal dependence of tropical lower-stratospheric temperature trends. *Atmospheric Chemistry and Physics*, 10(6), 2643–2653. <https://doi.org/10.5194/acp-10-2643-2010>
- Fu, Q., Solomon, S., Pahlevan, H. A., & Lin, P. (2019). Observed changes in Brewer–Dobson circulation for 1980–2018. *Environmental Research Letters*, 14(11), 114026. <https://doi.org/10.1088/1748-9326/ab4de7>
- Gao, P., Xu, X., & Zhang, X. (2015). Characteristics of the trends in the global tropopause estimated from COSMIC radio occultation data. *IEEE Transactions on Geoscience and Remote Sensing*, 53(12), 6813–6822. <https://doi.org/10.1109/TGRS.2015.2449338>
- Garcia, R. R., & Solomon, S. (1983). A numerical model of the zonally averaged dynamical and chemical structure of the middle atmosphere. *Journal of Geophysical Research*, 88(C2), 1379–1400. <https://doi.org/10.1029/JC088iC02p01379>
- Garfinkel, C. I., Aquila, V., Waugh, D. W., & Oman, L. D. (2017). Time-varying changes in the simulated structure of the Brewer–Dobson circulation. *Atmospheric Chemistry and Physics*, 17(2), 1313–1327. <https://doi.org/10.5194/acp-17-1313-2017>
- Garny, H., Dameris, M., Randel, W., Bodeker, G. E., & Deckert, R. (2011). Dynamically forced increase of tropical upwelling in the lower stratosphere. *Journal of the Atmospheric Sciences*, 68(6), 1214–1233. <https://doi.org/10.1175/2011JAS3701.1>
- Gleisner, H., Ringer, M. A., & Healy, S. B. (2022). Monitoring global climate change using GNSS radio occultation. *Npj Climate and Atmospheric Science*, 5(1), 1–4. <https://doi.org/10.1038/s41612-022-00229-7>
- Haynes, P., Hitchcock, P., Hitchman, M., Yoden, S., Hendon, H., Kiladis, G., et al. (2021). The influence of the stratosphere on the tropical troposphere. *Journal of the Meteorological Society of Japan. Ser. II*, 99(4), 803–845. <https://doi.org/10.2151/jmsj.2021-040>
- Hersbach, H., Bell, B., Berrisford, P., Biavati, G., Horányi, A., Muñoz-Sabater, J., et al. (2023). ERA5 monthly averaged data on single levels from 1940 to present. *Copernicus Climate Change Service (C3S) Climate Data Store (CDS)*. <https://doi.org/10.24381/cds.f17050d7>
- Hersbach, H., Bell, B., Berrisford, P., Hirahara, S., Horányi, A., Muñoz-Sabater, J., et al. (2020). The ERA5 global reanalysis. *Quarterly Journal of the Royal Meteorological Society*, 146(730), 1999–2049. <https://doi.org/10.1002/qj.3803>
- Hu, Y., Xia, Y., & Fu, Q. (2011). Tropospheric temperature response to stratospheric ozone recovery in the 21st century. *Atmospheric Chemistry and Physics*, 11(15), 7687–7699. <https://doi.org/10.5194/acp-11-7687-2011>

- Intergovernmental Panel on Climate Change (IPCC). (2023). Changing state of the climate system. In *Climate change 2021 – The Physical Science Basis: Working Group I contribution to the sixth assessment report of the intergovernmental Panel on climate change* (pp. 287–422). Cambridge University Press. <https://doi.org/10.1017/9781009157896.004>
- IPCC. (2021). In V. Masson-Delmotte, P. Zhai, A. Pirani, S. L. Connors, C. Péan, et al. (Eds.), *Climate change 2021: The physical science Basis. Contribution of Working Group I to the sixth assessment report of the intergovernmental Panel on climate change*. Cambridge University Press. In press. <https://doi.org/10.1017/9781009157896>
- Ivanciu, I., Matthes, K., Biastoch, A., Wahl, S., & Harlaß, J. (2022). Twenty-first-century southern Hemisphere impacts of ozone recovery and climate change from the stratosphere to the ocean. *Weather and Climate Dynamics*, 3(1), 139–171. <https://doi.org/10.5194/wcd-3-139-2022>
- Karoly, D., Cohen, J., Meehl, G., Mitchell, J., Oort, A., Stouffer, R., & Wetherald, R. (1994). An example of fingerprint detection of greenhouse climate change. *Climate Dynamics*, 10(1), 97–105. <https://doi.org/10.1007/BF00210339>
- Keeling, C. D., Bacastow, R. B., Bainbridge, A. E., Ekdahl, C. A., Jr., Guenther, P. R., Waterman, L. S., & Chin, J. F. S. (1976). Atmospheric carbon dioxide variations at Mauna Loa Observatory, Hawaii. *Tellus*, 28(6), 538–551. <https://doi.org/10.1111/j.2153-3490.1976.tb00701.x>
- Kessenich, H. E., Seppälä, A., & Rodger, C. J. (2023). Potential drivers of the recent large Antarctic ozone holes. *Nature Communications*, 14(1), 7259. <https://doi.org/10.1038/s41467-023-42637-0>
- Khaykin, S. M., Funatsu, B. M., Hauchecorne, A., Godin-Beckmann, S., Claud, C., Keckhut, P., et al. (2017). Postmillennium changes in stratospheric temperature consistently resolved by GPS radio occultation and AMSU observations. *Geophysical Research Letters*, 44(14), 7510–7518. <https://doi.org/10.1002/2017GL074353>
- Kuo, Y.-H., Wee, T.-K., Sokolovskiy, S., Rocken, C., Schreiner, W., Hunt, D., & Anthes, R. A. (2004). Inversion and error estimation of GPS radio occultation data. *Journal of the Meteorological Society of Japan. Ser. II*, 82(1B), 507–531. <https://doi.org/10.2151/jmsj.2004.507>
- Kursinski, E. R., Hajj, G. A., Schofield, J. T., Linfield, R. P., & Hardy, K. R. (1997). Observing Earth's atmosphere with radio occultation measurements using the global positioning system. *Journal of Geophysical Research*, 102(D19), 23429–23465. <https://doi.org/10.1029/97JD01569>
- Kuttippurath, J., & Nair, P. J. (2017). The signs of Antarctic ozone hole recovery. *Scientific Reports*, 7(1), 585. <https://doi.org/10.1038/s41598-017-00722-7>
- Ladstädter, F., Steiner, A. K., & Gleisner, H. (2023). Resolving the 21st century temperature trends of the upper troposphere–lower stratosphere with satellite observations. *Scientific Reports*, 13(1), 1306. <https://doi.org/10.1038/s41598-023-28222-x>
- Lan, X., Thoning, K. W., & Dlugokencky, E. J. (2022). Trends in globally-averaged CH₄, N₂O, and SF₆ determined from NOAA global monitoring laboratory measurements. Version 2024-08. <https://doi.org/10.15138/P8XG-AA1>
- Lawrence, Z. D., Abalos, M., Ayarzagüena, B., Barriopedro, D., Butler, A. H., Calvo, N., et al. (2022). Quantifying stratospheric biases and identifying their potential sources in subseasonal forecast systems. *Weather and Climate Dynamics*, 3(3), 977–1001. <https://doi.org/10.5194/wcd-3-977-2022>
- Leroy, S. S., Ao, C. O., & Verkhoglyadova, O. P. (2018). Temperature trends and anomalies in modern satellite data: Infrared sounding and GPS radio occultation. *Journal of Geophysical Research: Atmospheres*, 123(20), 11431–11444. <https://doi.org/10.1029/2018JD028990>
- Lim, E.-P., Hendon, H. H., Butler, A. H., Thompson, D. W. J., Lawrence, Z. D., Scaife, A. A., et al. (2021). The 2019 southern Hemisphere stratospheric polar vortex weakening and its impacts. *Bulletin of the American Meteorological Society*, 102(6), E1150–E1171. <https://doi.org/10.1175/BAMS-D-20-0112.1>
- Lin, P., & Fu, Q. (2013). Changes in various branches of the Brewer–Dobson circulation from an ensemble of chemistry climate models. *Journal of Geophysical Research: Atmospheres*, 118(1), 73–84. <https://doi.org/10.1029/2012JD018813>
- Livesey, N. J., Read, W. G., Froidevaux, L., Lambert, A., Santee, M. L., Schwartz, M. J., et al. (2021). Investigation and amelioration of long-term instrumental drifts in water vapor and nitrous oxide measurements from the Aura Microwave Limb Sounder (MLS) and their implications for studies of variability and trends. *Atmospheric Chemistry and Physics*, 21(20), 15409–15430. <https://doi.org/10.5194/acp-21-15409-2021>
- Mahieu, E., Chipperfield, M. P., Notholt, J., Redemann, T., Anderson, J., Bernath, P. F., et al. (2014). Recent northern Hemisphere stratospheric HCl increase due to atmospheric circulation changes. *Nature*, 515(7525), 104–107. <https://doi.org/10.1038/nature13857>
- Manabe, S., & Wetherald, R. T. (1967). Thermal equilibrium of the atmosphere with a given distribution of relative humidity. *Journal of the Atmospheric Sciences*, 24(3), 241–259. [https://doi.org/10.1175/1520-0469\(1967\)024<0241:teotaw>2.0.co;2](https://doi.org/10.1175/1520-0469(1967)024<0241:teotaw>2.0.co;2)
- Maycock, A. C. (2016). The contribution of ozone to future stratospheric temperature trends. *Geophysical Research Letters*, 43(9), 4609–4616. <https://doi.org/10.1002/2016GL068511>
- Maycock, A. C., Randel, W. J., Steiner, A. K., Karpechko, A. Y., Christy, J., Saunders, R., et al. (2018). Revisiting the mystery of recent stratospheric temperature trends. *Geophysical Research Letters*, 45(18), 9919–9933. <https://doi.org/10.1029/2018GL078035>
- McLandress, C., Jonsson, A. I., Plummer, D. A., Reader, M. C., Scinocca, J. F., & Shepherd, T. G. (2010). Separating the dynamical effects of climate change and ozone depletion. Part I: Southern Hemisphere stratosphere. *Journal of Climate*, 23(18), 5002–5020. <https://doi.org/10.1175/2010JCLI3586.1>
- McLandress, C., Shepherd, T. G., Scinocca, J. F., Plummer, D. A., Sigmond, M., Jonsson, A. I., & Reader, M. C. (2011). Separating the dynamical effects of climate change and ozone depletion. Part II: Southern Hemisphere troposphere. *Journal of Climate*, 24(6), 1850–1868. <https://doi.org/10.1175/2010JCLI3958.1>
- Meinshausen, M., Smith, S. J., Calvin, K., Daniel, J. S., Kainuma, M. L. T., Lamarque, J.-F., et al. (2011). The RCP greenhouse gas concentrations and their extensions from 1765 to 2300. *Climatic Change*, 109(1), 213–241. <https://doi.org/10.1007/s10584-011-0156-z>
- Ming, A., & Hitchcock, P. (2022). What contributes to the inter-annual variability in tropical lower stratospheric temperatures? *Journal of Geophysical Research: Atmospheres*, 127(1), e2021JD035548. <https://doi.org/10.1029/2021JD035548>
- Mitchell, D. M., Lo, Y. T. E., Seviour, W. J. M., Haimberger, L., & Polvani, L. M. (2020). The vertical profile of recent tropical temperature trends: Persistent model biases in the context of internal variability. *Environmental Research Letters*, 15(10), 1040b4. <https://doi.org/10.1088/1748-9326/ab9af7>
- Montzka, S. A., Dutton, G. S., Yu, P., Ray, E., Portmann, R. W., Daniel, J. S., et al. (2018). An unexpected and persistent increase in global emissions of ozone-depleting CFC-11. *Nature*, 557(7705), 413–417. <https://doi.org/10.1038/s41586-018-0106-2>
- Newman, P. A., & Nash, E. R. (2005). The unusual southern Hemisphere stratosphere winter of 2002. *Journal of the Atmospheric Sciences*, 62(3), 614–628. <https://doi.org/10.1175/JAS-3323.1>
- Newman, P. A., Nash, E. R., Kawa, S. R., Montzka, S. A., & Schauffler, S. M. (2006). When will the Antarctic ozone hole recover? *Geophysical Research Letters*, 33(12), L12814. <https://doi.org/10.1029/2005GL025232>
- Orbe, C., Wargan, K., Pawson, S., & Oman, L. D. (2020). Mechanisms linked to recent ozone decreases in the northern Hemisphere lower stratosphere. *Journal of Geophysical Research: Atmospheres*, 125(9), e2019JD031631. <https://doi.org/10.1029/2019JD031631>
- Perliski, L. M., Solomon, S., & London, J. (1989). On the interpretation of seasonal variations of stratospheric ozone. *Planetary and Space Science*, 37(12), 1527–1538. [https://doi.org/10.1016/0032-0633\(89\)90143-8](https://doi.org/10.1016/0032-0633(89)90143-8)

- Ploeger, F., & Garny, H. (2022). Hemispheric asymmetries in recent changes in the stratospheric circulation. *Atmospheric Chemistry and Physics*, 22(8), 5559–5576. <https://doi.org/10.5194/acp-22-5559-2022>
- Polvani, L. M., Abalos, M., Garcia, R., Kinnison, D., & Randel, W. J. (2018). Significant weakening of brewer-dobson circulation trends over the 21st century as a consequence of the Montreal protocol. *Geophysical Research Letters*, 45(1), 401–409. <https://doi.org/10.1002/2017GL075345>
- Polvani, L. M., Wang, L., Abalos, M., Butchart, N., Chipperfield, M. P., Dameris, M., et al. (2019). Large impacts, past and future, of ozone-depleting substances on brewer-dobson circulation trends: A multimodel assessment. *Journal of Geophysical Research: Atmospheres*, 124(13), 6669–6680. <https://doi.org/10.1029/2018JD029516>
- Randel, W. J., Polvani, L., Wu, F., Kinnison, D. E., Zou, C.-Z., & Mears, C. (2017). Troposphere-Stratosphere temperature trends derived from satellite data compared with ensemble simulations from WACCM. *Journal of Geophysical Research: Atmospheres*, 122(18), 9651–9667. <https://doi.org/10.1002/2017JD027158>
- Randel, W. J., & Wu, F. (2015). Variability of zonal mean tropical temperatures derived from a decade of GPS radio occultation data. *Journal of the Atmospheric Sciences*, 72(3), 1261–1275. <https://doi.org/10.1175/JAS-D-14-0216.1>
- Read, W. G., Lambert, A., Bacmeister, J., Cofield, R. E., Christensen, L. E., Cuddy, D. T., et al. (2007). Aura microwave limb sounder upper tropospheric and lower stratospheric H₂O and relative humidity with respect to ice validation. *Journal of Geophysical Research (Atmospheres)*, 112(D24), D24S35. <https://doi.org/10.1029/2007JD008752>
- Rigby, M., Park, S., Saito, T., Western, L. M., Redington, A. L., Fang, X., et al. (2019). Increase in CFC-11 emissions from eastern China based on atmospheric observations. *Nature*, 569(7757), 546–550. <https://doi.org/10.1038/s41586-019-1193-4>
- Robertson, F., Revell, L. E., Douglas, H., Archibald, A. T., Morgenstern, O., & Frame, D. (2023). Signal-to-noise calculations of emergence and De-Emergence of stratospheric ozone depletion. *Geophysical Research Letters*, 50(16), e2023GL104246. <https://doi.org/10.1029/2023GL104246>
- Santer, B. D., Po-Chedley, S., Zhao, L., Zou, C.-Z., Fu, Q., Solomon, S., et al. (2023). Exceptional stratospheric contribution to human fingerprints on atmospheric temperature. *Proceedings of the National Academy of Sciences*, 120(20), e2300758120. <https://doi.org/10.1073/pnas.2300758120>
- Santer, B. D., Wigley, T. M. L., Mears, C., Wentz, F. J., Klein, S. A., Seidel, D. J., et al. (2005). Amplification of surface temperature trends and variability in the tropical atmosphere. *Science*, 309(5740), 1551–1556. <https://doi.org/10.1126/science.1114867>
- Scherllin-Pirscher, B., Steiner, A. K., Anthes, R. A., Alexander, M. J., Alexander, S. P., Biondi, R., et al. (2021). Tropical temperature variability in the UTLS: New insights from GPS radio occultation observations. *Journal of Climate*, 34(8), 2813–2838. <https://doi.org/10.1175/JCLI-D-20-0385.1>
- Shangguan, M., Wang, W., & Jin, S. (2019). Variability of temperature and ozone in the upper troposphere and lower stratosphere from multi-satellite observations and reanalysis data. *Atmospheric Chemistry and Physics*, 19(10), 6659–6679. <https://doi.org/10.5194/acp-19-6659-2019>
- Shepherd, T. G. (2007). Transport in the middle atmosphere. *Journal of the Meteorological Society of Japan. Ser. II*, 85B, 165–191. <https://doi.org/10.2151/jmsj.85B.165>
- Solomon, S., Dube, K., Stone, K., Yu, P., Kinnison, D., Toon, O. B., et al. (2022). On the stratospheric chemistry of midlatitude wildfire smoke. *Proceedings of the National Academy of Sciences*, 119(10), e2117325119. <https://doi.org/10.1073/pnas.2117325119>
- Solomon, S., Garcia, R. R., Rowland, F. S., & Wuebbles, D. J. (1986). On the depletion of antarctic ozone. *Nature*, 321(6072), 755–758. <https://doi.org/10.1038/321755a0>
- Solomon, S., Ivy, D., Gupta, M., Bandoro, J., Santer, B., Fu, Q., et al. (2017). Mirrored changes in Antarctic ozone and stratospheric temperature in the late 20th versus early 21st centuries. *Journal of Geophysical Research: Atmospheres*, 122(16), 8940–8950. <https://doi.org/10.1002/2017JD026719>
- Solomon, S., Ivy, D. J., Kinnison, D., Mills, M. J., Neely, R. R., & Schmidt, A. (2016). Emergence of healing in the Antarctic ozone layer. *Science*, 353(6296), 269–274. <https://doi.org/10.1126/science.aao0061>
- Solomon, S., Stone, K., Yu, P., Murphy, D. M., Kinnison, D., Ravishankara, A. R., & Wang, P. (2023). Chlorine activation and enhanced ozone depletion induced by wildfire aerosol. *Nature*, 615(7951), 259–264. <https://doi.org/10.1038/s41586-022-05683-0>
- SPARC. (2022). SPARC reanalysis intercomparison project (S-RIP) final report. In M. Fujiwara, G. L. Manney, L. J. Gray, & J. S. Wright (Eds.), *SPARC report No. 10*, WCRP-6/2021. <https://doi.org/10.17874/800dee57d13>
- Steiner, A. K., Hunt, D., Ho, S.-P., Kirchengast, G., Mannucci, A. J., Scherllin-Pirscher, B., et al. (2013). Quantification of structural uncertainty in climate data records from GPS radio occultation. *Atmospheric Chemistry and Physics*, 13(3), 1469–1484. <https://doi.org/10.5194/acp-13-1469-2013>
- Steiner, A. K., Ladstädter, F., Ao, C. O., Gleisner, H., Ho, S.-P., Hunt, D., et al. (2020). Consistency and structural uncertainty of multi-mission GPS radio occultation records. *Atmospheric Measurement Techniques*, 13(5), 2547–2575. <https://doi.org/10.5194/amt-13-2547-2020>
- Steiner, A. K., Ladstädter, F., Randel, W. J., Maycock, A. C., Fu, Q., Claud, C., et al. (2020). Observed temperature changes in the troposphere and stratosphere from 1979 to 2018. *Journal of Climate*, 33(19), 8165–8194. <https://doi.org/10.1175/JCLI-D-19-0998.1>
- Stiller, G. P., Fierli, F., Ploeger, F., Cagnazzo, C., Funke, B., Haenel, F. J., et al. (2017). Shift of subtropical transport barriers explains observed hemispheric asymmetry of decadal trends of age of air. *Atmospheric Chemistry and Physics*, 17(18), 11177–11192. <https://doi.org/10.5194/acp-17-11177-2017>
- Stiller, G. P., von Clarmann, T., Haenel, F., Funke, B., Glathor, N., Grabowski, U., et al. (2012). Observed temporal evolution of global mean age of stratospheric air for the 2002 to 2010 period. *Atmospheric Chemistry and Physics*, 12(7), 3311–3331. <https://doi.org/10.5194/acp-12-3311-2012>
- Stocker, M., Ladstädter, F., & Steiner, A. K. (2021). Observing the climate impact of large wildfires on stratospheric temperature. *Scientific Reports*, 11(1), 22994. <https://doi.org/10.1038/s41598-021-02335-7>
- Stocker, M., Steiner, A. K., Ladstädter, F., Foelsche, U., & Randel, W. J. (2024). Strong persistent cooling of the stratosphere after the Hunga eruption. *Communications Earth and Environment*, 5(1), 1–11. <https://doi.org/10.1038/s43247-024-01620-3>
- Stone, K. A., Solomon, S., Kinnison, D. E., & Mills, M. J. (2021). On recent large antarctic ozone holes and ozone recovery metrics. *Geophysical Research Letters*, 48(22), e2021GL095232. <https://doi.org/10.1029/2021GL095232>
- Sweeney, A. (2025). Software and data for recent warming of southern Hemisphere subtropical lower stratosphere and antarctic ozone healing. In *Seattle*. Zenodo. <https://doi.org/10.5281/zenodo.15785195>
- Thompson, D. W. J., & Wallace, J. M. (2000). Annular modes in the extratropical circulation. Part I: month-To-month variability. *Journal of Climate*, 13(5), 1000–1016. [https://doi.org/10.1175/1520-0442\(2000\)013<1000:amitec>2.0.co;2](https://doi.org/10.1175/1520-0442(2000)013<1000:amitec>2.0.co;2)
- Tseng, H.-H., & Fu, Q. (2017). Temperature control of the variability of tropical tropopause layer cirrus clouds. *Journal of Geophysical Research: Atmospheres*, 122(20), 11062–11075. <https://doi.org/10.1002/2017JD027093>

- Vallis, G. K., Zurita-Gotor, P., Cairns, C., & Kidston, J. (2015). Response of the large-scale structure of the atmosphere to global warming. *Quarterly Journal of the Royal Meteorological Society*, 141(690), 1479–1501. <https://doi.org/10.1002/qj.2456>
- Vergados, P., Ao, C. O., Mannucci, A. J., & Kursinski, E. R. (2021). Quantifying the tropical upper tropospheric warming amplification using radio occultation measurements. *Earth and Space Science*, 8(2), e2020EA001597. <https://doi.org/10.1029/2020EA001597>
- Villamayor, J., Iglesias-Suarez, F., Cuevas, C. A., Fernandez, R. P., Li, Q., Abalos, M., et al. (2023). Very short-lived halogens amplify ozone depletion trends in the tropical lower stratosphere. *Nature Climate Change*, 13(6), 554–560. <https://doi.org/10.1038/s41558-023-01671-y>
- Wallace, J. M., Panetta, R. L., & Estberg, J. (1993). Representation of the equatorial stratospheric quasi-biennial oscillation in EOF phase space. *Journal of the Atmospheric Sciences*, 50(12), 1751–1762. [https://doi.org/10.1175/1520-0469\(1993\)050<1751:ROTESQ>2.0.CO;2](https://doi.org/10.1175/1520-0469(1993)050<1751:ROTESQ>2.0.CO;2)
- Wang, P., Solomon, S., Santer, B., Kinnison, D., Fu, Q., Stone, K., et al. (2025). Fingerprinting the robust recovery of antarctic ozone. *Nature*. (in press). <https://doi.org/10.21203/rs.3.rs-4876981/v1>
- Wang, P., Solomon, S., & Stone, K. (2023). Stratospheric chlorine processing after the 2020 Australian wildfires derived from satellite data. *Proceedings of the National Academy of Sciences*, 120(11), e2213910120. <https://doi.org/10.1073/pnas.2213910120>
- Weyland, F., Hoor, P., Kunkel, D., Birner, T., Plöger, F., & Turhal, K. (2025). Long-term changes in the thermodynamic structure of the lowermost stratosphere inferred from reanalysis data. *Atmospheric Chemistry and Physics*, 25(2), 1227–1252. <https://doi.org/10.5194/acp-25-1227-2025>
- Wolter, K., & Timlin, M. S. (2011). El Niño/Southern Oscillation behaviour since 1871 as diagnosed in an extended multivariate ENSO index (MEIext). *International Journal of Climatology*, 31(7), 1074–1087. <https://doi.org/10.1002/joc.2336>
- World Meteorological Organization (WMO). (2011). *Scientific assessment of ozone depletion: 2010*. World Meteorological Organization.
- World Meteorological Organization (WMO), Executive Summary. (2022). *Scientific assessment of ozone depletion: 2022*. GAW Report No. 278. WMO.56
- Xia, Y., Xu, W., Hu, Y., & Xie, F. (2020). Southern-Hemisphere high-latitude stratospheric warming revisit. *Climate Dynamics*, 54(3), 1671–1682. <https://doi.org/10.1007/s00382-019-05083-7>
- Yook, S., Thompson, D. W. J., & Solomon, S. (2022). Climate impacts and potential drivers of the unprecedented antarctic ozone holes of 2020 and 2021. *Geophysical Research Letters*, 49(10), e2022GL098064. <https://doi.org/10.1029/2022GL098064>
- Yulaeva, E., Holton, J. R., & Wallace, J. M. (1994). On the cause of the annual cycle in tropical lower-stratospheric temperatures. *Journal of the Atmospheric Sciences*, 51(2), 169–174. [https://doi.org/10.1175/1520-0469\(1994\)051<169:OTCOTA>2.0.CO;2](https://doi.org/10.1175/1520-0469(1994)051<169:OTCOTA>2.0.CO;2)
- Zambri, B., Solomon, S., Thompson, D. W. J., & Fu, Q. (2021). Emergence of southern Hemisphere stratospheric circulation changes in response to ozone recovery. *Nature Geoscience*, 14(9), 638–644. <https://doi.org/10.1038/s41561-021-00803-3>
- Zhang, J., Wang, P., Kinnison, D., Solomon, S., Guan, J., Stone, K., & Zhu, Y. (2024). Stratospheric chlorine processing after the unprecedented Hunga Tonga eruption. *Geophysical Research Letters*, 51(17), e2024GL108649. <https://doi.org/10.1029/2024GL108649>
- Zolghadrshojaee, M., Tegtmeier, S., Davis, S. M., & Pilch Kedzierski, R. (2024). Variability and long-term changes in tropical cold-point temperature and water vapor. *Atmospheric Chemistry and Physics*, 24(12), 7405–7419. <https://doi.org/10.5194/acp-24-7405-2024>
- Zuev, V. V., Maslennikova, E. A., Savelieva, E. S., & Pavlinsky, A. V. (2024). Sensitivity of the antarctic polar vortex to temperature changes in the lower subtropical stratosphere. *Atmospheric and Oceanic Optics*, 37(1), 99–102. <https://doi.org/10.1134/S1024856023700124>